Electro-kinetics of charged-sphere suspensions explored by integral low-angle super-heterodyne laser Doppler velocimetry

OPEN ACCESS
IOP PUBLISHING
JOURNAL OF PHYSICS: CONDENSED MATTER
J. Phys.: Condens. Matter **24** (2012) 464109 (19pp)
doi:10.1088/0953-8984/24/46/464109

Electro-kinetics of charged-sphere suspensions explored by integral low-angle super-heterodyne laser Doppler velocimetry

Thomas Palberg[1], **Tetyana Köller**[1], **Bastian Sieber**[1], **Holger Schweinfurth**[1], **Holger Reiber**[1] **and Gerhard Nägele**[2]

[1] Institut für Physik, Johannes Gutenberg Universität, D-55128 Mainz, Germany
[2] Forschungszentrum Jülich GmbH, IFF, D-52425 Jülich, Germany

E-mail: palberg@uni-mainz.de

Received 8 March 2012
Published 31 October 2012
Online at stacks.iop.org/JPhysCM/24/464109

Abstract
We investigated the flow behaviour of colloidal charged-sphere suspensions using a newly designed integral low-angle super-heterodyne laser Doppler velocimetry instrument, which combines the advantages of several previous approaches. Sample conditions ranged from strong electrostatic interactions with pronounced short-range order to individual particles with no spatial correlations. The obtained power spectra correspond to diffusion broadened velocity distributions across the complete sample cross section. The excellent performance of the instrument is highlighted in detail by the example of electro-kinetic flow of suspensions in a closed cell of a rectangular cross section. We demonstrate the excellent performance of our approach with the example of electro-phoretic–electro-osmotic experiments, showing that a comprehensive flow characterization becomes possible by analysing the measured electro-kinetic mobilities, the flow-profile, an effective diffusion coefficient and the integrated scattering density. We briefly discuss present limitations, possible extensions and interesting applications in other fields.

(Some figures may appear in colour only in the online journal)

1. Introduction

Charged colloidal spheres, if subjected to an external electric field E, will acquire a stationary drift velocity $v_e = \mu E$ against the surrounding solvent. For the case of infinitely thin double layers (i.e. in the Smoluchowski-limit [1] $\kappa a \gg 1$, with particle radius a and screening parameter κ) the particle mobility, μ_e, is connected to the electrostatic potential, ζ, defined at the plane of zero shear as $\mu_e = \varepsilon_0 \varepsilon_r \zeta / \eta$, where ε_0 and ε_r are the dielectric permittivities of vacuum and solvent, respectively, and η is the solvent viscosity. The same expression applies also to the electro-osmotic mobility, $\mu_{eo} = u_{eo}/E$, with u_{eo} as the solvent mobility along an infinitely extended, planar and charged wall [2]. A larger number of approximate analytical expressions and numerical schemes have also been developed to cover other values of κa [3–7], and to include more complex effects like surface conductivity [8–10] and electric double layer overlap [11, 12]. Recent theoretical developments based on spherical cell models also approach the strictly salt-free case considering as micro-ions only the particle-released counter-ions [13, 14] as well as the realistic salt-free suspension additionally including water auto-protolysis and dissociation of dissolved CO_2 [15]. Experiments on model latex or silica spheres show that in most cases μ_e decreases with increasing salt concentration and in addition shows a pronounced dependence on the particle concentration [16]. In the limit of isolated particles, the particle mobilities are very small and independent of the particle size [17–19]. With increasing particle concentration, the mobility reveals a complex behaviour. It first increases

logarithmically [20–22], then passes a plateau and finally decreases logarithmically [23, 24].

The final decrease of μ_e in the strongly interacting, fluid-like or crystalline ordered state is understood theoretically as the decrease of the ζ-potential with increasing salinity, i.e. with increasing concentration of counter-ions. In fact, μ_e starts its descent when the number of counter-ions becomes roughly ten times larger than the number of salt ions [24]. This part of the concentration dependence of μ_e can be approximately described using an ad hoc combination of charge renormalization theory [25–28] and the standard electro-kinetic model of O'Brien and White [3] in which electrostatic particle interactions are neglected. In charge renormalization theory, the effective charge of a spherical (or rod-like) colloid is reduced in the saturation regime to a saturation value, Z_{eff}, practically independent of the bare charge, Z, due to the condensation of counter-ions in a thin layer on the particle surface. The salinity and the effective screening parameter at saturation are determined by the concentrations of added salt and uncondensed counter-ions. Both are experimentally accessible in conductivity experiments [29, 30]. A decreasing mobility is also found in computer simulations of strictly salt-free suspensions [31]. Still, only when realistic salt-free conditions are considered is a transition of μ_e from a plateau value at moderate particle concentration to a logarithmic decrease at larger concentrations observed in theory [15, 32].

The counter-intuitive increase of the colloid mobility with particle concentration observed at low particle concentrations is not fully understood to date. However, it is experimentally documented both in deionized systems and in systems of enlarged salinity [16, 22, 33]. Interestingly, the transition from a mobility increasing with concentration to a concentration-independent one occurs as the electric double layers start overlapping and a fluid-like order starts to evolve, i.e. when the static structure factor develops a visible primary maximum [33]. For the low concentration regime, simulations, theory and the ad hoc model noted before predict a wrong dependence of μ_e on particle concentration. Since, at very low particle concentration, counter-ion condensation vanishes so that the ζ-potential is controlled by the much larger bare charge [28, 34, 35], all these approaches predict a continuous increase of the mobility upon dilution [31, 24], which clearly is at variance with the experimental observations.

This study analyses the electro-kinetics of several charged-sphere suspensions of different concentrations and salinities. This includes samples of pronounced fluid-like order, several weakly ordered samples at intermediate interaction strengths, but also unstructured samples at very low concentrations. We employ a recently introduced low-angle, reference beam super-heterodyne Doppler velocimetry setup for integral measurements across the complete cross section of a closed sample cell [24]. This instrument combines the reference beam integral measurement of [36] (allowing measurement of the complete flow-profile in a single measurement) with super-heterodyning [37, 38] (allowing separation of the heterodyne part of the power spectrum from the homodyne part and low frequency noise) and a low scattering angle (allowing signals independent of the system structure to be obtained by exploiting the dominance of incoherent scattering in strongly interacting suspensions) [39, 40]. The method has been already successfully used to study the flow of colloidal crystals under the influence of an electric field [23, 41], but so far it has not been systematically characterized for its use in quantitative electro-kinetic measurements in fluid-like ordered or disordered states. Therefore, we will show that this method allows for facile quantitative determination of flow-profiles, particle electro-phoretic and electro-osmotic mobilities, μ_e and μ_{eo}, and the effective diffusion coefficient, D_{eff}, as well as the spectral power, A. All these quantities contain complementary information about the system flow properties. We anticipate that such detailed measurements will also be helpful for the study of other flow situations, in particular for flows driven by hydrostatic pressure differences, or in sedimentation experiments.

We will discuss the observed characteristic dependences of the extracted quantities on the experimental parameters, namely particle concentration and salinity, which control the structure of the electric double layer, the degree of double layer overlap, and the formation of short-range order. Our data are consistent with previous measurements, but they also provide interesting new experimental findings, e.g. an increase of the spectral power and of the effective diffusivity with increased field strength. In addition, we find a significant difference between the electro-osmosis along a planar wall and the electro-phoresis of colloidal spheres, even for the same surface chemistry. While the measured particle mobility show the known increase with increasing particle concentration, followed by a plateau of the mobility at strongly interacting conditions and pronounced fluid-like order, the electro-osmotic mobility appears to be independent of the particle concentration.

The paper is organized as follows. In section 2 we first briefly sketch the experimental setup and discuss the expected flow-profiles. We then recall the corresponding light scattering theory and finally describe the samples and the preparation techniques employed. Section 3 starts with a test of the assumptions underlying the derivation of the theoretical Doppler spectra and here in particular of the assumed flow-profile also under the condition of strong particle interactions. It further addresses the systematic field-strength dependence of the spectral power and the effective diffusivity, as well as the different electro-kinetic responses of wall and particles to a changing concentration of spheres. Based on these results, we then discuss the general performance of the super-heterodyne method for characterizing the flow of colloidal suspensions in differently ordered states. We end the paper with a short conclusion.

2. Experimental details

2.1. Integral reference beam mode super-heterodyne Doppler velocimetry

Colloidal particle velocities were obtained from a home-built laser Doppler velocimetry instrument. The setup is shown

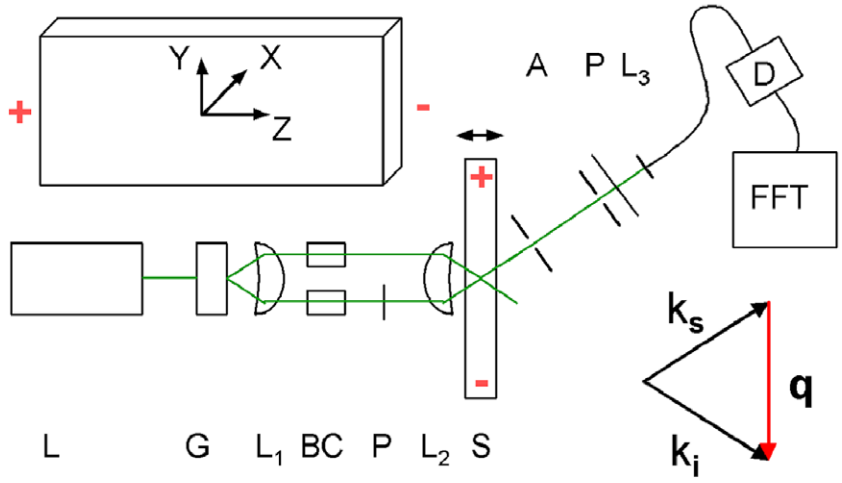

Figure 1. The super-heterodyne reference beam mode laser Doppler velocimetry instrument. Top: sketch of the rectangular flow-through cell and the coordinate system used. The plus and minus signs indicate the electrodes used to induce the combined electro-phoretic–electro-osmotic flow experiments. Middle: top view scheme of the super-heterodyne experiment (for a detailed description see text). Bottom right: definition of the scattering wave vector, **q**.

schematically in figure 1. The beam of a Nd:YAG laser (L, $\lambda_0 = 532$ nm) of circular frequency $\omega_0 \sim 10^{15}$ Hz is split into two beams, a reference beam (r) and an illuminating beam (i), using a beam splitter. Alternatively also a sinusoidal transmission grid (G) can be used (Sine Patterns, Pittsford NY). The two beams are made parallel by a lens L_1. Each beam passes through a Bragg-cell (BC) and is frequency shifted by the circular frequencies $\omega_i = 80.002$ MHz and $\omega_r = 80.000$ MHz, with the larger frequency shift realized for the illuminating beam (upper beam in figure 1). This results in a positive relative Bragg-shift, $\Delta\omega_B = \omega_i - \omega_r$, in the circular frequency corresponding to $\Delta f_B = \Delta\omega_B/2\pi = (2000 \pm 5)$ Hz. The beams are redirected into the sample cell (S) by a lens, L_2, where they cross in the suspension under an angle of $\Theta_S = (10°-18°)$. (Note that in figure 1 we show the beam propagation in air.) In addition to a polarizer (P), the detector side optics includes a set of apertures (A) to define the observed sample volume. For our so-called integral measurements, light scattered off the particles in the complete illuminated part of the sample is received within the acceptance angle of a grin lens defining the scattering vector **q**. The lens is mounted at the inlet of an optical fibre leading to a photomultiplier used to record the intensity (D). The scattering vector $\mathbf{q} = \mathbf{k}_i - \mathbf{k}_s$, where $\mathbf{k}_i$ and $\mathbf{k}_s$ are the wave vectors of the illuminating and scattered beams, is parallel to the applied field direction (cf figure 1). In the present sign convention, **q** is proportional to the momentum transfer from the photon to the scattering particle. Its modulus is given by $q = (4\pi\upsilon_S/\lambda_0)\sin(\Theta_S/2) = (4\pi/\lambda_0)\sin(\Theta/2)$, where υ_S is the index of refraction of the solvent and Θ is the beam crossing angle in air. We note that light scattered by a particle j moving with a velocity $\mathbf{v}_j$ is Doppler-shifted by the circular frequency $\omega_D = -\mathbf{q}\cdot\mathbf{v}(x, y)$ where the velocity could be a function of the position. The frequency shift, ω_D, is positive, if the particle velocity shares an obtuse angle with the scattering vector, $\mathbf{q} = q\hat{\mathbf{z}}$, where $\hat{\mathbf{z}}$ is the unit vector in the z-direction. Hence, a positive Doppler shift corresponds to particles moving towards the detector.

The reference beam is also directed into the fibre and superimposed with the scattered light. It therefore acts as a local oscillator, and gives rise to beats in the observed intensity which are analysed by a fast Fourier transform analyzer (Ono Sokki DS2000, Compumess, Germany) to yield the power spectrum as a function of frequency, $f = \omega/2\pi$. To obtain a decent signal to noise ratio, typically some 200–2000 subsequent spectra were averaged. The averaged spectra were background corrected. In addition we corrected for an experimentally observed peak at $\Delta\omega/2\pi = 2$ kHz, which is not considered in our theory. This peak results from the beat of reference beam light and parasitic stray light scattered from the illumination beam at the glassware surfaces. The experimental spectra were replaced by a straight line across the peak region (typically a few hertz), thus cutting out the peak but retaining an estimate of the spectral power originating from particle motion. Except when explicitly noted, all experimental spectra shown below are treated in this way.

2.2. Flow-profile and velocity distribution

As sketched in figure 1 on the upper left, the origin of our coordinate system is at the cell centre with $x \parallel d$, $y \parallel h$ and $z \parallel l$. Measurements were performed in closed quartz cells of rectangular cross section with depth × height $= 2d \times 2h =$ 1 mm × 10 mm (Rank Bros., Bottisham, Cambridge, UK). The optical part of the cell length, l, spanned some 40 mm. The effective platinum electrode distance was $L \approx 80$ mm, and was determined precisely before each measurement series from calibration with an electrolyte dilution series. During the measurements, the electrode chambers were sealed against the remaining preparation circuit by electromagnetic valves closed upon stop of pumping. To avoid accumulation of particles at the electrodes, alternating square-wave fields of strength up to $E_{MAX} = U/L = 80$ V cm^{-1} were applied. To ensure fully developed stationary flows, field switching

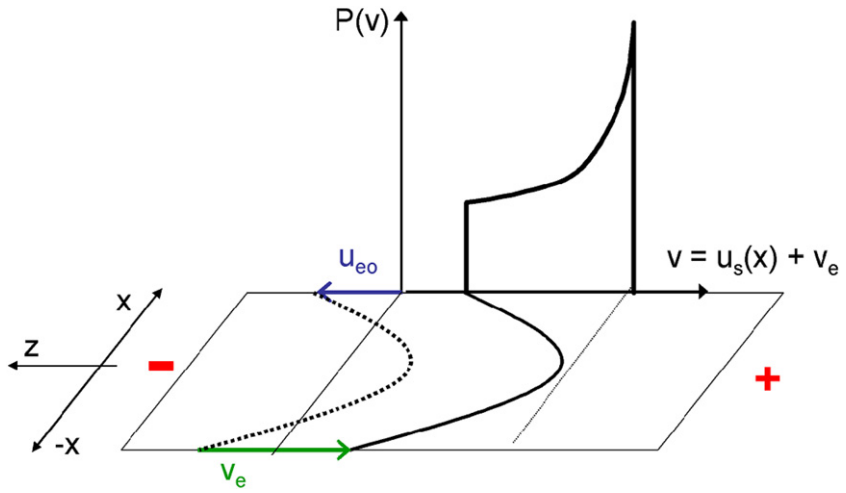

Figure 2. Velocities in an electro-phoretic experiment performed in a closed rectangular cell as shown in figure 1. Horizontal x–z mid-plane: laboratory-frame velocity profiles, $v(x) = v(x; y = 0)$ and $u_s(x) = u_s(x; y = 0)$, of particles and solvent, respectively. Vertical plane: corresponding probability density, $P(v)$, of finding a particle of given velocity, v. In our setup, the external field $\mathbf{E}$, $\mathbf{u}_{eo}$ and $\mathbf{q}$ are aligned with the positive z-axis, whereas $\mathbf{v}_e$ points into the negative z-direction.

frequencies of $f_{AC} = (0.05-0.2)$ Hz were used. Measurement intervals were restricted to one field direction, starting 2 s after field reversal and ending 1 s before the next field reversal.

As sketched in figure 2, the application of an electric field in a closed cell geometry induces an electro-osmotic flow-profile of the incompressible solvent. The static electric field, $\mathbf{E}$, points into the positive z-direction. Surface-released cations in the thin double layer at the negatively charged cell walls move towards the negative electrode with a velocity $u_{eo} > 0$ pointing along the positive z-axis and drag some solvent along with them. A central solvent backflow in the direction of the negative z-axis assures volume conservation (cf figure 2). The stationary, electro-osmotically induced solvent flow, $u_s(x, y)$, can be calculated numerically [42], but for the mid-plane flow an analytical approximation has also been given by Komagata [43]. For a cell with aspect $K = h/d$, the mid-plane ($y = 0$) solvent velocity profile is given by

$$u_s(x, y = 0) = u_{eo}\left[1 - 3\left(\frac{1 - x^2/d^2}{2 - 384/(\pi^5 K)}\right)\right]. \qquad (1)$$

This quadratic and unidirectional profile is sketched in figure 2. Note that the mean velocity, given as the integral of $u_s(x, y)$ over the *complete* cross section, is zero in the laboratory frame due to volume conservation of the incompressible solvent. Note further that also the mid-plane cross section averaged shear rate, $\langle \mathrm{d}u_s(x, y = 0)/\mathrm{d}x\rangle$, is zero. The stretching of the flow-profile depends on the electro-osmotic velocity, u_{eo}, and hence on the surface chemistry of the cell and the applied field strength, E. Typically, prior to filling, our cells were treated with Deconex®, and thoroughly rinsed repeatedly with acetone and with doubly distilled water. This resulted in an electro-osmotic mobility of about 6 (μm s^{-1}) (V cm^{-1})$^{-1}$, equivalent to a zeta-potential of roughly 150 mV, in agreement with literature values. Occasionally, we observed contamination with low solubility substances resisting the washing procedure. Then the cells were heated to 1000 °C in an open reducing flame or treated with 1 M H_2SO_4 prior to an extended washing procedure. The latter cells showed appreciably larger electro-osmotic velocities. An example in case is seen in the height dependent flow-profile measurements in figure 7.

Superimposed on this solvent flow-profile is the electro-phoretic motion of charged colloidal particles relative to the solvent, with the electro-phoretic velocity $\mathbf{v}_e = \mu_e\mathbf{E}$. The constant electro-phoretic velocity, $v_e < 0$, of the negatively charged colloids points in the negative z-direction towards the positive electrode. The resulting flow-profile in the laboratory frame, $v(x, y) = v_e + u_s(x, y)$, is thus equal to the solvent profile shifted in the negative direction by the constant amount $|v_e|$. The integral of $v(x, y)$ over the *complete* cross section yields v_e.

Also drawn schematically in figure 2 is the particle velocity distribution, $P(v) = P(v(\mu_e E = v_e, \mu_{eo}E = u_{eo}))$, where $P(v)\,\mathrm{d}v$ is the fraction of colloids with velocity in an infinitesimal interval $\mathrm{d}v$ around v. Assuming the number density, n, of colloidal particles to remain homogeneous and unperturbed by the electro-osmotic flow, one has $P(v) \propto n\,\mathrm{d}x/\mathrm{d}v$ [36]. The shape of $P(v)$ reflects the parabolic flow-profile with a sharp peak at the maximal (midcell) velocity. For sufficiently large K, the mid-plane P-average (centre of mass) velocity $\langle v\rangle_P \approx v_e$. For systems with constant electro-osmotic velocity but a distribution of electro-phoretic mobilities, μ_e, the corresponding velocity distribution function is obtained by averaging $P(v)$ over the mobility distribution, under the assumption that the partial number densities of particle sub-systems of equal mobility remain spatially homogeneous. In this case an additional broadening of the velocity distribution is obtained which increases with increasing field strength [36, 44, 45].

2.3. Light scattering theory

The theoretical background for our experiments is based on earlier work on homo- and heterodyning techniques

in dynamic light scattering [40, 46–48]. The theory for conventional heterodyne Doppler velocimetry using an integral reference beam setup was outlined in [36]. In a forthcoming paper [45], we describe the full super-heterodyne theory, including a discussion, for the present setup, of the importance of decorrelation effects such as Taylor dispersion arising in sheared solvents [49] and a rigorous treatment of electro-phoretic mobility polydispersity. Here we only briefly summarize the main theoretical points.

Our experiment determines the power spectrum, $C_{\mathrm{shet}}(\mathbf{q}, \omega)$, which is the time Fourier transformation of the mixed-field intensity autocorrelation function, $C_{\mathrm{shet}}(\mathbf{q}, \tau)$, and is given by

$$C_{\mathrm{shet}}(\mathbf{q}, \omega) = \frac{1}{\pi} \int_{-\infty}^{\infty} \mathrm{d}\tau \, \cos(\omega\tau) C_{\mathrm{shet}}(\mathbf{q}, \tau) \tag{2}$$

with circular frequency ω and correlation time τ. For a scattered light field of Gaussian statistics the latter quantity is given as

$$\begin{aligned} C_{\mathrm{shet}}(\mathbf{q}, \tau) = {} & (I_{\mathrm{r}} + \langle I_{\mathrm{S}}(\mathbf{q}) \rangle)^2 + 2 I_{\mathrm{r}} \langle I_{\mathrm{S}}(\mathbf{q}) \rangle \\ & \times \mathrm{Re}[\hat{g}_E(\mathbf{q}, \tau) \exp(-\mathrm{i}\omega_{\mathrm{B}}\tau)] \\ & + \langle I_{\mathrm{S}}(\mathbf{q}) \rangle^2 |\hat{g}_E(\mathbf{q}, \tau)|^2. \end{aligned} \tag{3}$$

Here, I_{r} is the reference beam intensity, $\langle I_{\mathrm{S}}(\mathbf{q}) \rangle$ is the time-averaged scattered intensity, and $\hat{g}_E(\mathbf{q}, \tau) = g_E(\mathbf{q}, \tau)/\langle I_{\mathrm{S}}(\mathbf{q}) \rangle$ is the normalized field autocorrelation function.

To proceed, we first consider the simplest case of a system of (i) zero macroscopic solvent flow, (ii) a suspension consisting of strictly monodisperse spheres of spatially uniform and constant electro-phoretic drift velocity, $\mathbf{v} = \mathbf{v}_{\mathrm{e}}^0 = \mu_{\mathrm{e}}^0 \mathbf{E}$, which are (iii) non-interacting (superscript 0). We then investigate the effects of relaxing these assumptions, step by step.

Assuming independence of diffusive motion and electro-phoretic drift we can easily obtain $C_{\mathrm{shet}}(\mathbf{q}, \tau)$ for a system of strictly monodisperse, non-interacting spheres of spatially uniform and constant electro-phoretic drift velocity in a quiescent solvent. It is given by

$$\begin{aligned} C_{\mathrm{shet}}^0(\mathbf{q}, \tau) = {} & (I_{\mathrm{r}} + \langle I_{\mathrm{S}}^0(\mathbf{q}) \rangle)^2 + 2 I_{\mathrm{r}} \langle I_{\mathrm{S}}^0(\mathbf{q}) \rangle \\ & \times \cos((\omega_{\mathrm{B}} - \mathbf{q} \cdot \mathbf{v}_e^0)\tau) \exp(-q^2 D^0 |\tau|) \\ & + \langle I_{\mathrm{S}}^0(\mathbf{q}) \rangle^2 \exp(-q^2 D^0 |\tau|). \end{aligned} \tag{4}$$

Here we used $\langle I_{\mathrm{S}}^0(\mathbf{q}) \rangle = I_0 n f^2(q) S(q)$, where I_0 denotes an apparative function reflecting the optical details of the experiment, while n and $f(q)$ denote the particle number density and single-particle scattering amplitude for strictly monodisperse spheres, respectively. For non-interacting particles $S(q) = 1$. D^0 denotes the single sphere translational diffusion coefficient at infinite dilution. $C_{\mathrm{shet}}^0(\mathbf{q}, \tau)$ consists of three additive terms: a constant background term, a damped cosine function in τ related to the heterodyne contribution, and an exponentially decaying function related to the homodyne contribution caused by the self-beating of the scattered light. The last term contains no information on the drift velocity. The super-heterodyne power spectrum for strictly monodisperse, non-interacting spheres of constant and spatially uniform electro-phoretic drift velocity in a quiescent solvent then follows from equation (3) as

$$\begin{aligned} C_{\mathrm{shet}}^0(\mathbf{q}, \omega) = {} & [I_{\mathrm{r}} + \langle I_{\mathrm{S}}^0(\mathbf{q}) \rangle]^2 \delta(\omega) + \frac{I_{\mathrm{r}} \langle I_{\mathrm{S}}^0(\mathbf{q}) \rangle}{\pi} \\ & \times \left[\frac{q^2 D_0}{(\omega + [\omega_{\mathrm{B}} - \mathbf{q} \cdot \mathbf{v}_{0,\mathrm{e}}])^2 + (q^2 D_0)^2} \right. \\ & \left. + \frac{q^2 D_0}{(\omega - [\omega_{\mathrm{B}} - \mathbf{q} \cdot \mathbf{v}_{0,\mathrm{e}}])^2 + (q^2 D_0)^2} \right] \\ & + \frac{\langle I_{\mathrm{S}}^0(\mathbf{q}) \rangle^2}{\pi} \frac{2 q^2 D_0}{\omega^2 + (2 q^2 D_0)^2}. \end{aligned} \tag{5}$$

It is the sum of an irrelevant singular term at $\omega = 0$, two symmetrically shifted Lorentzians of half-width at half-height, $q^2 D_0$, centred at $\omega = \pm[\omega_{\mathrm{B}} - \mathbf{q} \cdot \mathbf{v}_{\mathrm{e}}^0]$, which constitute the interesting heterodyne (Doppler) part, and an un-shifted Lorentzian of double-sized half-width at half-height $2q^2 D_0$, centred at $\omega = 0$. The two heterodyne Lorentzians are Bragg-shifted away from the origin by $\omega_{\mathrm{B}} - \mathbf{q} \cdot \mu_{\mathrm{e}}^0 \mathbf{E}$, so that they can be distinguished from the central homodyne Lorentzian. In addition, the sign of μ_{e} can be inferred.

In equation (5), a quiescent solvent was considered. Following [36], the power spectrum for a distribution of velocities, $P(v)$, under stationary flow for non-interacting, strictly monodisperse particles can be calculated approximately as the superposition of Lorentzians

$$C_{\mathrm{shet}}^0(\mathbf{q}, \omega) \approx \int \mathrm{d}v \, P(v) C_{\mathrm{shet}}^0(\mathbf{q}, \omega, \mu_{\mathrm{e}}^0 \mathbf{E}, D_0). \tag{6}$$

As detailed in [36], this superposition approximation does not include Taylor-dispersion effects on $C_{\mathrm{shet}}^0(\mathbf{q}, \tau)$, arising from local shear-flow particle advection in a non-quiescent solvent (see also [47, 50, 51]). Thus it applies precisely to arbitrary flow-profiles only in the limit of $D_0 \to 0$. However, differently from various shear-flow experiments, where Taylor dispersion plays a decisive role [52–55], the electro-osmotic solvent flow according to equation (1) at the fields strengths employed in the present study is so weak, and the involved Peclet numbers are so small, that equation (6) should become an excellent approximation. In the case of non-negligible Taylor dispersion, however, one can expect a stronger broadening for those parts of the power spectrum which stem from cell regions of larger shear rates. In the present case of electro-kinetic flow in a closed cell, we would anticipate an enhanced broadening of the low frequency region of the spectra stemming from low velocity, high-shear regions close to the cell wall (cf figure 2).

The theoretically expected spectral shape for the complete super-heterodyne spectrum for a system of negatively charged, strictly monodisperse, non-interacting spheres subjected to a homogeneous electric field in a closed cell geometry and measured at midcell height is sketched in figure 3. Note that the spectrum is symmetric with respect to the origin, as a consequence of stationarity. In section 3, we will therefore only consider the restricted frequency range containing the positive heterodyne Doppler contribution.

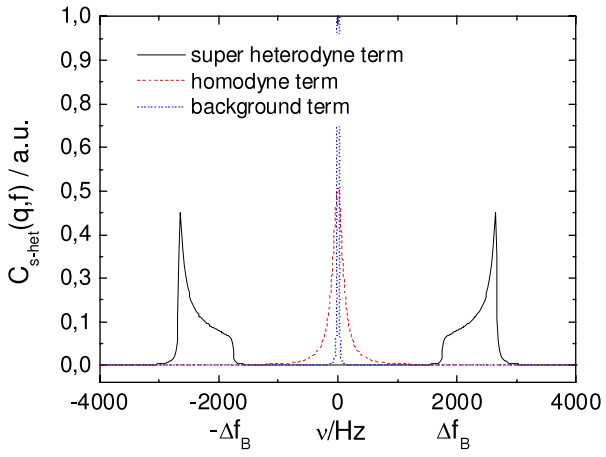

Figure 3. Sketch of the theoretically expected complete super-heterodyne power spectrum for mobility and size monodisperse, negatively charged colloidal particles subjected to a homogeneous electric field in a closed cell geometry and measured at midcell height. The spectrum is calculated using equations (5), (6) and (1), on neglecting possible particle mobility distributions, velocity fluctuations and Taylor dispersion. The interesting information about the spatially uniform particle drift velocity is contained only in the symmetric heterodyne part (solid line), which is shifted with respect to the homodyne term (dashed) and the background term (dotted). Note that the shape of the positively shifted heterodyne part reflects the diffusion broadened velocity distribution sketched in figure 2.

Next, we relax the condition of strictly monodisperse spheres, but again consider a quiescent solvent and a homogeneous electric field. For polydisperse systems with given distributions of μ_e and D_0, averaging over these distributions does not affect the frequency shifts of the centres of the two heterodyne Lorentzian wings, but it leads to two additional kinds of symmetric broadening of these wings that grow with increasing polydispersity. We note that in particular the broadening due to a mobility polydispersity increases with increased electric field strength, E. We note further that also temporal fluctuations of the drift velocity, $\mathbf{v}_e(t) = \mathbf{v}_{0,e} + \Delta\mathbf{v}_e(t)$, will, according to recent simulations [56], translate into a field-strength dependent symmetric broadening. While the heterodyne part in these cases is not an exact Lorentzian any more, it still may be approximated by a Lorentzian curve, but with an effective diffusion coefficient, D_{eff}, somewhat larger than D_0 that increases with electric field strength. For a non-quiescent solvent and a known velocity distribution $P(v)$, we again can use equation (6) to calculate the superposition integral for the approximated Lorentzians, characterized now by D_{eff} and $\mathbf{v}_e$.

So far, we have only considered non-interacting particle systems. For polydisperse systems of electrostatically interacting particles in a stationary solvent flow, and subjected to a homogeneous electric field, $g_E(\mathbf{q}, \tau)$ is proportional to the steady-state measurable dynamic structure factor, $S_M(\mathbf{q}, \tau)$ [40]. For systems of dominant optical polydispersity but essentially no interaction polydispersity, $S_M(\mathbf{q}, \tau)$ can be calculated to good accuracy in the so-called decoupling approximation. This condition is decently fulfilled by our copolymer latex particles with a low size polydispersity of $s \leq 0.05$ and considerable optical inhomogeneity, and also for the optically homogeneous silica spheres with their moderate size polydispersity of $s \leq 0.1$. Considering the steady-state *self*-intermediate scattering function, $G(\boldsymbol{q}, \tau)$, and the interaction-monodisperse steady-state coherent dynamic structure factor, $S(\mathbf{q}, \tau)$, the steady-state measurable dynamic structure factor, $S_M(\mathbf{q}, \tau)$, and hence $g_E(\mathbf{q}, \tau)$, can then be approximated by a weighted superposition of a coherent and an incoherent scattering contribution according to

$$g_E(\mathbf{q}, \tau) = I_0 n\overline{f^2(q)} S_M(\mathbf{q}, \tau) \approx I_0 n\overline{f^2(q)}[9s^2 G(\mathbf{q}, \tau) + S(\mathbf{q}, \tau)], \quad (7)$$

where, again, I_0 is an apparative function reflecting the optical details of the experiment, n is the particle number density, and $\overline{f^2(q)}$ is the size-distribution averaged square of the form amplitude. For sufficiently large correlation times, τ, and sufficiently large length scales, $2\pi/q$, we may further approximate the steady-state $G(\boldsymbol{q}, \tau)$ by its Markovian limit, i.e. by the expression for non-interacting systems, but with the single-particle electro-phoretic velocity, $\mathbf{v}_{0,e}$ (or $\mathbf{v}_e(t)$, if fluctuations are considered), being replaced by the long-time average velocity, $\bar{\mathbf{v}}_e$, which may differ from $\mathbf{v}_{e,0}$ due to the particle interactions. Furthermore, the single sphere diffusion coefficient at infinite dilution, D^0, is replaced by an effective diffusion coefficient, D_{eff}, which, as before, is influenced by mobility polydispersity and/or velocity fluctuations, but now also reflects the particle interactions. For vanishing electric field strength, D_{eff} should therefore be identified with the long-time self-diffusion coefficient.

An expression for the coherent part, $S(\mathbf{q}, \tau)$, for interacting suspensions in an external electric field, and in the presence of an electro-osmotic shear flow, is not known to date. However, for non-interacting systems, where $S(q) = 1$, $S(\mathbf{q}, \tau)$ is equal to $G(\mathbf{q}, \tau)$. With increasing interactions, the low-q values of $S(q)$ (relating to the isothermal osmotic compressibility) decrease until the incoherent scattering contribution dominates and the conditions to safely neglect $S(\mathbf{q}, \tau)$ are fulfilled. That is, for strongly interacting particle systems, observation on timescales of 100 ms and longer, and at a small scattering wave number well below that of the principal peak of the static structure factor, we should then be able to measure self-diffusion and electro-kinetic motion of individual particles which only differ in their optical properties. Hence our experiment may be viewed as a tracer experiment without explicit tracers. This viewpoint may, of course, be invalidated by shear- and/or electric field-induced density fluctuations. It also loses its strictness for weakly interacting suspensions where the osmotic compressibility is not low.

In our electro-kinetic experiments we investigate polydisperse charged spheres suspended in a non-quiescent solvent and under different interaction conditions. According to the above discussion, experimental Doppler spectra should be well described by a theoretical expression of the positive heterodyne part of the spectra calculated using equations (1) and (5) in equation (6), with the appropriate replacements used. Deviations from the predicted spectral shape are to

be expected, e.g., for field- or flow-induced accumulation of particles in the cell centre or at the cell walls [57], and for shear thinning effects [58, 59] in strongly interacting systems including colloidal crystals [41]. A comparison of the experimentally obtained spectral shape to the theoretical prediction combined with a comparison of the electro-phoretic velocities from a measurement at mid-plane height to the cross section averaged drift velocity therefore allows for a sensitive test of the validity of the electro-osmotic flow-profile of equation (1) under conditions of strong particle interactions.

With equation (1) validated, we can obtain $\bar{\mathbf{v}}_e$, $\bar{\mathbf{u}}_{eo}$, D_{eff} and the integrated spectral density A as the four independent physical parameters, from fits of the theoretical expression to the experimental Doppler spectra. These quantities relate (approximately) to the centre of mass of $P(v)$, the width of $P(v)$, the symmetric diffusion-like broadening and the signal strength. We can then check the systematic dependence of these four parameters on the adjusted experimental conditions. The integrated spectral density, A, of the heterodyne part of the spectral density is proportional to $I_r\langle I_S(\mathbf{q})\rangle = I_r I_0 n\overline{f^2(q)}(9s^2 + S(q))$. It thus should scale with n, and it should be larger in the non- and weakly interacting states than in the strongly interacting state of the system. Additional field- or flow-induced density fluctuations on length scales $2\pi/q$ may become observable through an increased steady-state $S(\mathbf{q}, \tau)$, describing density correlations in such a driven system. Further, one may check for a field-strength dependence or a shear rate dependence of D_{eff}. As mentioned above, an increase of D_{eff} with increased field can be expected for mobility polydispersity [36, 44], for a temporally fluctuating electro-phoretic drift velocity, $\mathbf{v}_e \neq$ const. [56], or for Taylor dispersion in a strong local electro-osmotic shear flow at the container walls [49]. In the latter case we would further expect a characteristic frequency dependence of the broadening of the Doppler spectra, with the largest broadening present for the lowest Doppler frequencies stemming from regions close to the cell wall. The zero-field extrapolated value of D_{eff} is anticipated to be large and to relate to collective diffusion as long as the power spectrum is dominated by coherent scattering, while it should be smaller than D_0 when the incoherent signal dominates and D_{eff} relates to the *self*-diffusion coefficient [40]. Finally, from the field dependence of the long-time average electro-kinetic velocities both electro-kinetic mobilities are inferred by linear fits.

2.4. Samples and sample preparation

Several species of charged spheres were used. The three latex species comprised poly-*n*-butylacrylamide-polystyrene (PnBAPS) 35:65 copolymer particles, and were a kind gift of BASF, Ludwigshafen. Their size polydispersity is only small to moderate, but due to their chemical inhomogeneity these particle species show strong incoherent scattering. The particle size distribution of the PnPAPS68 suspensions deduced from ultracentrifugation is shown in figure 4. The PnBAPS68 particles have a mean diameter of $\sigma = 2a = 68$ nm and a standard deviation in the particle sizes of $s \approx 0.05$ with a slight asymmetry. The

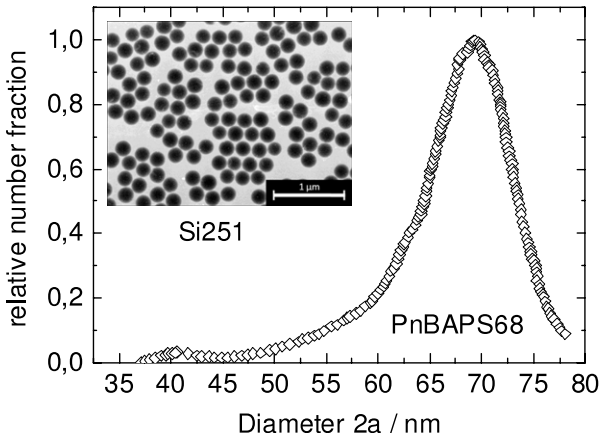

Figure 4. Particle size distribution from ultracentrifugation for PnBAPS68. The inset shows a TEM picture of Si251. The scale bar is 1 μm.

effective charge from conductance measurements is $Z_{eff} = (450 \pm 20)e^-$ [60]. PnBAPS68 has been extensively used in previous investigations. As we have run out of stock of this species most of the systematic data were obtained from the replacement species PnBAPS70, which has a mean diameter of $2a = 70$ nm and a slightly lower polydispersity. The effective charge of this latter species is $Z_{eff} = (425 \pm 10)e^-$. Aqueous suspensions of both species could be investigated without significant multiple scattering up to large particle concentrations, where the systems crystallize.

The third species, PnBAPS359 ($2a = 359$ nm, $s = 0.03$, $Z_{eff} \approx 10^3 e^-$), is particularly well suited for measurements at very low particle densities. It has been investigated in the non- to moderately interacting fluid-like ordered regime. Working at larger particle concentrations was inhibited by the onset of strong multiple scattering. The optically homogeneous Si251 silica spheres have a mean diameter of $2a = 251$ nm and a relative standard deviation in the size distribution of $s = 0.08$ as determined from TEM measurements (cf figure 4, inset). Their incoherent scattering contribution is smaller, but also here the low concentration regime with isolated particles was readily accessible.

All samples were prepared from pre-cleaned stock suspensions of large particle concentrations stored over a mixed-bed ion exchanger (Amberlite, Room & Haas, France). The desired concentrations were adjusted by precise dilution with Milli-Q-grade water, and under control of the particle number density, n, via static light scattering. The suspensions were filled in a closed Teflon® tubing circuit for final conditioning. The tubing system connects an ion exchange chamber, a reservoir under an inert Ar atmosphere (to add further suspension, CO_2 or solvent), and a set of different cells for simultaneous measurements under identical conditions. These usually comprise (i) a conductivity experiment, (ii) a cell for static light scattering, and (iii) the flow-through cell for the velocity measurements. Details of the preparation circuit used are given elsewhere [61, 62]. We only note here that residual impurity concentrations on the level of the self-dissociation product of water are reached within a

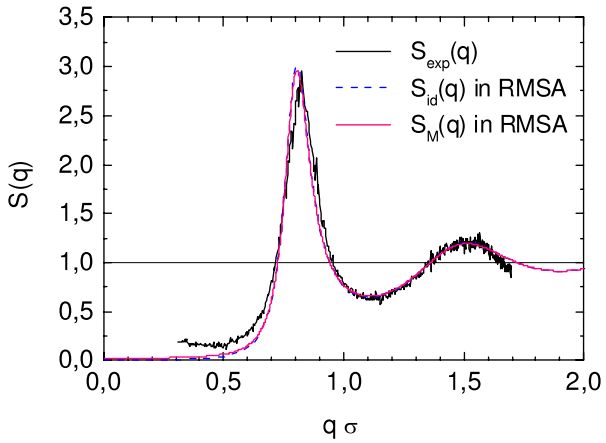

Figure 5. Background corrected experimental structure factor, $S_{\rm exp}(q)$, for a quiescent, deionized suspension of PnBAPS68 at $n = 5.1\ \mu{\rm m}^{-3}$ (corresponding to a volume fraction of $\Phi = n(4\pi/3)a^3 = 8.38 \times 10^{-4}$) compared to the theoretical, decoupling approximated, measurable structure factor, $S_{\rm M}(q)$, for $\sigma = 2a = 68$ nm and a polydispersity of $s = 0.05$, and an ideal one-component $S_{\rm id}(q)$, obtained from RMSA calculations using a DLVO-type screened Coulomb pair potential. To match the peak height of the theoretical $S_{\rm M}(q)$ to the experimental $S_{\rm exp}(q)$ an effective charge of $Z = 557e^-$ was used. Note that all $S(q)$ are practically q-independent, for the range around $q^* = q\sigma \approx 0.4$ probed in the flow experiments.

few hours. For measurements at elevated salt concentrations, gaseous CO_2 was added after complete deionization, and continued cycling under bypassing the ion exchange column ensured homogenization. The salt concentration was controlled by conductivity measurements [30] and the particle concentration by static light scattering, both with a residual uncertainty of about 1%. The preparation method is therefore fast and assures good reproducibility of the *in situ* controlled interaction parameters.

The obtained structures were analysed by a standard static light scattering experiment. The experimental structure factor was obtained from division of the (background corrected) scattered mean intensity of an ordered suspension by the (background corrected) scattered intensity from a non-interacting suspension of the same species (at a salt concentration of $c = 4 \times 10^{-4}$ mol l^{-1}) weighted with the dilution ratio $n_{\text{non-interacting}}/n_{\text{ordered}}$. The measured static structure factor, $S_{\rm exp}(q)$, for a field-free deionized suspension of PnBAPS68 is shown in figure 5. Fits of a theoretical decoupling approximation structure factor, $S_{\rm M}(q)$, for the experimentally determined size polydispersity of $s = 0.05$ and an ideal one-component $S_{\rm id}(q)$ are also shown in figure 4. Both were obtained from the standard rescaled mean-spherical approximation (RMSA) using a DLVO-type screened Coulomb pair potential [40]. Both functions describe the data overall quite well. Note, however, that our electro-kinetic velocity measurements were conducted at $q^* = q\sigma \approx 0.4$, which lies is in the low-q region of the structure factor. There, we find $S_{\rm M}(q^*) = 0.034 \gg S_{\rm id}(q^*) = 0.003$, showing that the incoherent contribution dominates $S_{\rm M}(q, \tau)$ at sufficiently small q (cf equation (7)). In particular, for the latex systems, $S_{\rm exp}(q^*)$ lies significantly above $S_{\rm M}(q^*)$, which is the theoretical estimate for particles with optical polydispersity deriving solely from size polydispersity. The additional experimentally observed incoherent contribution for the latex spheres is attributed to their optical inhomogeneity, which is not accounted for in this estimate.

3. Results

3.1. Spectral shape and flow-profiles

Given that the mid-plane flow-profile of equation (1) is a sufficiently accurate approximation, the spectral shape is a fingerprint of the flow-profile and may serve as a sensitive measure of deviations from Newtonian flow behaviour in strongly interacting suspensions. An obvious example is the case where the cohesion of a colloidal crystal counteracts the development of a parabolic particle flow-profile. But also in the fluid-like ordered state, deviations from the expected spectral shape are, in principle, possible. They are, e.g., expected for shear thinning systems [58, 59] or for shear-induced particle accumulation either at the cell walls or in the cell centre [57]. Before proceeding to any quantitative evaluation of the measured spectra, we first have to check that (i) the shape of our Doppler spectra is independent of the experimental conditions and that (ii) equation (1) gives the quantitatively correct description of the particle flow also for conditions of strongly interacting particles.

Figures 6(a)–(f) show power spectra obtained on two deionized suspensions of PnBAPS68. The data in figures 6(a)–(c) were taken close to the freezing transition ($n_{\rm F} \approx 5\ \mu{\rm m}^{-3}$). Those of figures 6(d)–(f) were obtained in a state which was more dilute, but still well ordered. With increasing field strength, the Doppler spectra in (a) and (c) get more elongated due to the increased electro-osmotic flow. The positions of their centres of mass shift to larger frequencies due to the increased mean electro-phoretic velocity of the particles. Also, the effective diffusion coefficient, $D_{\rm eff}$, increases with increasing field strength. Its value extrapolated to zero applied field is 1.2×10^{-12} cm^2 s^{-1} for $n = 0.47\ \mu{\rm m}^{-3}$, which is significantly below the Stokes–Einstein value of $D_0 = 6.30 \times 10^{-12}$ cm^2 s^{-1}, which is used here to approximate the single sphere diffusion coefficient at infinite dilution, D^0. To compare the spectral forms, we subtract the Bragg-shift frequency and divide the resulting relative frequencies by the applied field strength, while the intensity is multiplied by E. The so-scaled spectra in (b) and (d) clearly show an increase in spectral density with increasing field strength. In (c) and (f), we further normalize the spectra to equal integrated spectral density. One readily notes that the spectral forms remain unchanged upon changes in field strength. This implies (i) an unaltered flow-profile and (ii) that the intensity increase in the Doppler spectra with increasing E is an effect affecting all particles in an equal manner. This in turn excludes a relation of the intensity increase to the spatially varying shear state of the system.

Figure 7(a) demonstrates that a Doppler spectrum measured at the mid-plane of the cell can be excellently fitted by equation (6), using the $P(v)$ derived from the

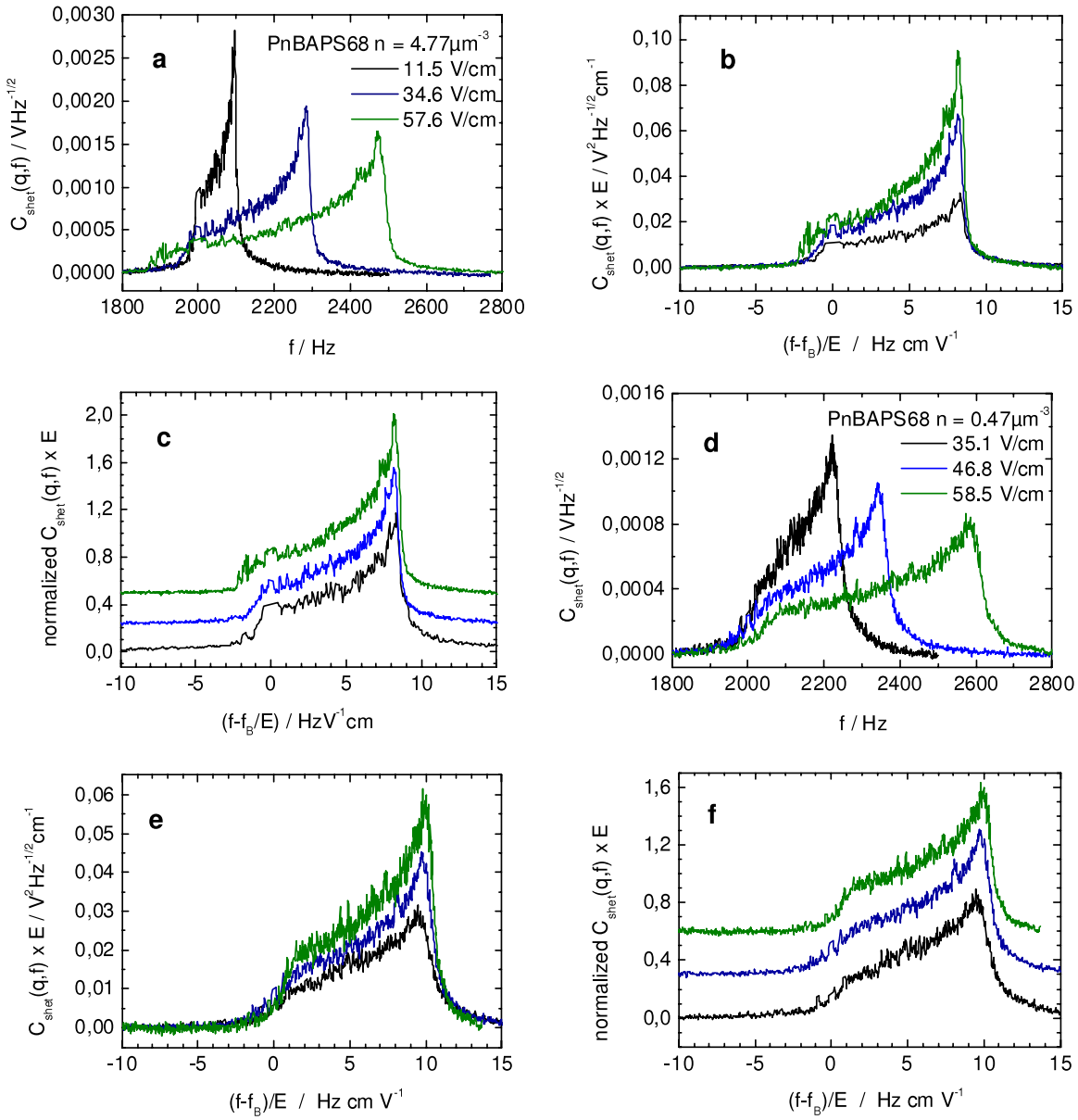

Figure 6. Selected Doppler spectra of deionized suspensions of PnBAPS68 for different electric field strengths, E, as indicated, and $q = 4.4\ \mu\text{m}^{-1}$. (a)–(c): $n = 4.77\ \mu\text{m}^{-3}$; (d)–(f): $n = 0.47\ \mu\text{m}^{-3}$; (a), (d): raw power spectra; (b), (e): scaled spectra; (c), (f): scaled spectra normalized to equal integrated spectral density, and shifted for clarity. With increasing field strength, the spectral power increases. The spectral shapes hardly change.

approximate Komagata mid-plane flow-profile according to equation (1), with $K = 10$. For the considered strongly interacting suspension of PnBAPS68 at $n = 3.7\ \mu\text{m}^{-1}$ and $c = 0.2\ \mu\text{mol l}^{-1}$ subjected to a field of $E = 57.6\ \text{V cm}^{-1}$, we obtain the following fit results: an electro-phoretic velocity of $\mathbf{v}_\text{e} = (-435 \pm 23)\ \mu\text{m s}^{-1}$, an electro-osmotic velocity of $u_\text{eo} = (584.5 \pm 41)\ \mu\text{m s}^{-1}$, an effective diffusion coefficient of $D_\text{eff} = (7.3 \pm 0.8)\ \mu\text{m}^2\ \text{s}^{-2}$ and an integrated spectral power of $A = (0.32 \pm 0.02)\ \text{V Hz}^{1/2}$. For the typical quality of the spectral data obtained from a measurement duration of 60 s, the relative uncertainty in the velocities from an individual experiment is well below 10%. Due to the presence of upper and lower walls, the flow-profile at mid-height slightly deviates from an ideal parabola (cf equation (1)), and the mid-plane averaged velocity, $\langle v \rangle_x$, corresponding to the median of the distribution does not exactly coincide with the electro-phoretic velocity, $\mathbf{v}_\text{e}$.

This becomes more obvious for the Doppler spectra taken in height dependent measurements on the same sample which are shown in figure 6(b). For height values $y < 4$ mm the spectral shape is hardly changed, while closer to the top wall the width of the spectral feature shrinks significantly. Note that the position of the low frequency end of the spectral feature remains practically unchanged with changing y, reflecting the constant velocity at the cell walls, while the high frequency end moves to lower frequencies, and the median is approaching $\mathbf{u}_\text{eo} + \mathbf{v}_\text{e}$. The x-averaged velocities, $\langle \mathbf{v}(y) \rangle_x$, are plotted in figure 7(c). Going inward from the

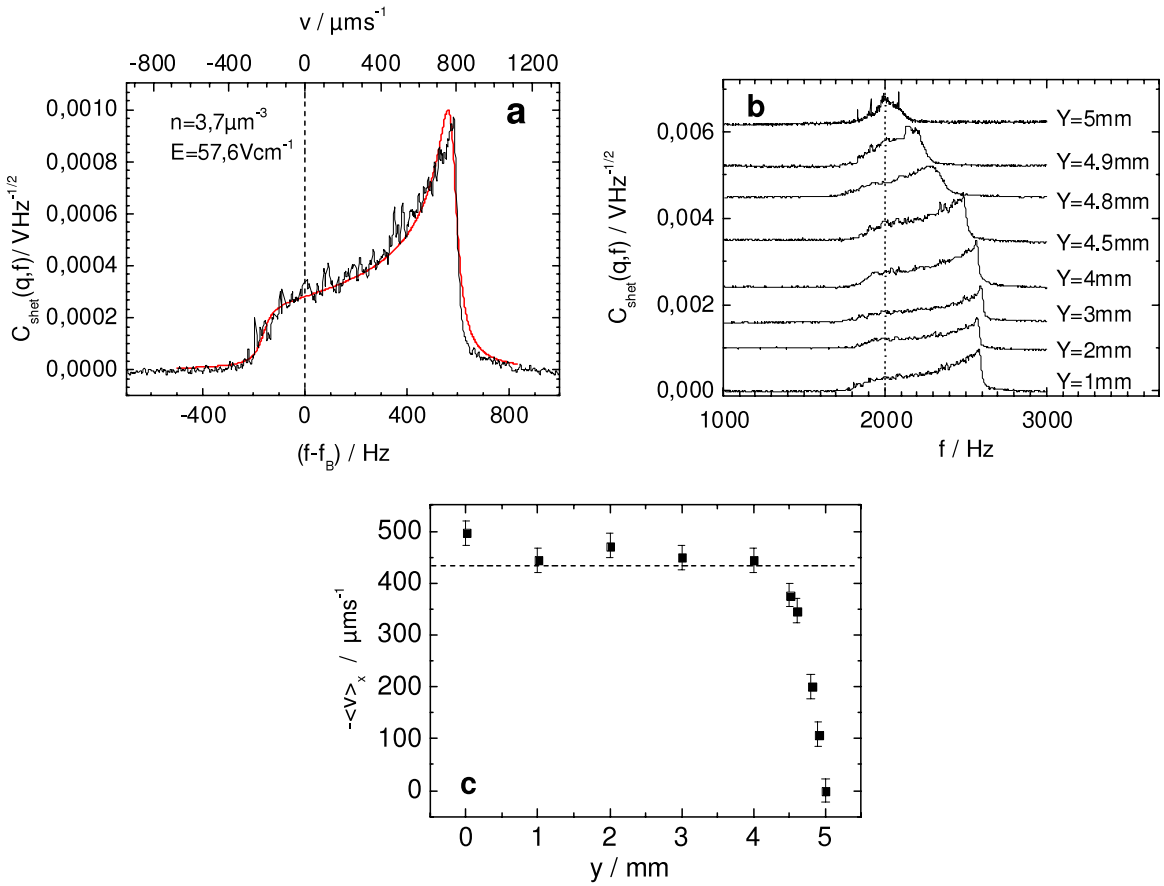

Figure 7. (a) Mid-plane Doppler spectrum of a deionized suspension of PnBAPS68 obtained under the conditions as indicated and $q = 5.1\ \mu\text{m}^{-1}$, and fitted using equations (4)–(6) (red curve). The fit parameters obtained are $\mathbf{v}_e = (-435 \pm 23)\ \mu\text{m s}^{-1}$; $u_{eo} = (584.5 \pm 41)\ \mu\text{m s}^{-1}$; $D_{eff} = (7.3 \pm 0.8)\ \mu\text{m}^2\ \text{s}^{-1}$; $A = (0.32 \pm 0.02)\ \text{VHz}^{1/2}$. (b) Doppler spectra determined at different heights y as indicated. The spectra are shifted for clarity. The vertical dotted line indicates the Bragg-shift frequency f_B. Note the continuous change of the spectral shape. (c) x-averaged (centre of mass) velocities obtained for the spectra in (b). Their double average, $\langle\langle v(y)\rangle_x\rangle_y = -430.9\ \mu\text{m s}^{-1}$ (dashed line), coincides well with the value obtained for $\mathbf{v}_e$ from the fit in (a), $\mathbf{v}_e = (-435 \pm 23)\ \mu\text{m s}^{-1}$, but it is considerably below the mid-plane average velocity of $\langle v(y = 0)\rangle_x = -496.1\ \mu\text{m s}^{-1}$.

cell top at $y = 5$ mm the velocity first increases steeply, but for $y < 4$ mm only mildly. Due to volume conservation, the double-averaged velocity, $\langle\langle \mathbf{v}(y)\rangle_x\rangle_y$, should coincide with $\mathbf{v}_e$, if equation (1) is a valid approximation. The value obtained from figure 7(c), $\langle\langle \mathbf{v}(y)\rangle_x\rangle_y = -430.9\ \mu\text{m s}^{-1}$, indeed is considerably smaller than the average mid-plane velocity, $\langle \mathbf{v}(y = 0)\rangle_x = (-496.1)\ \mu\text{m s}^{-1}$, but coincides well with the value obtained from the fit which is $\mathbf{v}_e = (-435 \pm 23)\ \mu\text{m s}^{-1}$.

Our analysis demonstrates that (i) as for non-interacting systems [36], also under conditions of strong electrostatic interaction the Komagata flow-profile of equation (1) is quantitatively retained, (ii) shear thinning effects known from pressure driven flows are absent, and also particle accumulation is not observable, (iii) the spectra may hence safely be interpreted as reflecting mid-plane velocity distributions, and (iv) the relevant velocities $\mathbf{v}_e$ and $\mathbf{u}_{eo}$ can therefore be obtained reliably from a single measurement at mid-plane. This last result is corroborated by the observation that the experimentally determined electro-phoretic velocities for strongly interacting systems are in excellent agreement both with state-of-the-art analytical calculations [12], and with combined Monte Carlo and Lattice-Boltzmann computer simulations on the primitive model level [31, 63]. The simultaneous determination of electro-osmotic velocities in a single light scattering experiment is here performed for the first time.

We proceed to less ordered systems. We start with the transition range of strong to weak electrostatic interactions for a fluid-like ordered system of small particles. Here, much care was taken to measure all data under identical optical conditions, e.g. equal illumination intensity and sensitivity settings of the detector. The scaled Doppler spectra of PnBAPS70 for different n and c are shown in figures 8(a)–(f). They are sorted from left to right by decreasing height of the principal peak of the unsheared static structure factor (from 2.3 to 1.2), which may serve as a qualitative measure of the decreasing interaction strength and spatial correlation. The intensity increase with increasing field strength is still seen in the samples with $n = 1.85\ \mu\text{m}^{-3}$, but vanishes for the more dilute samples. It is practically absent for the very dilute systems.

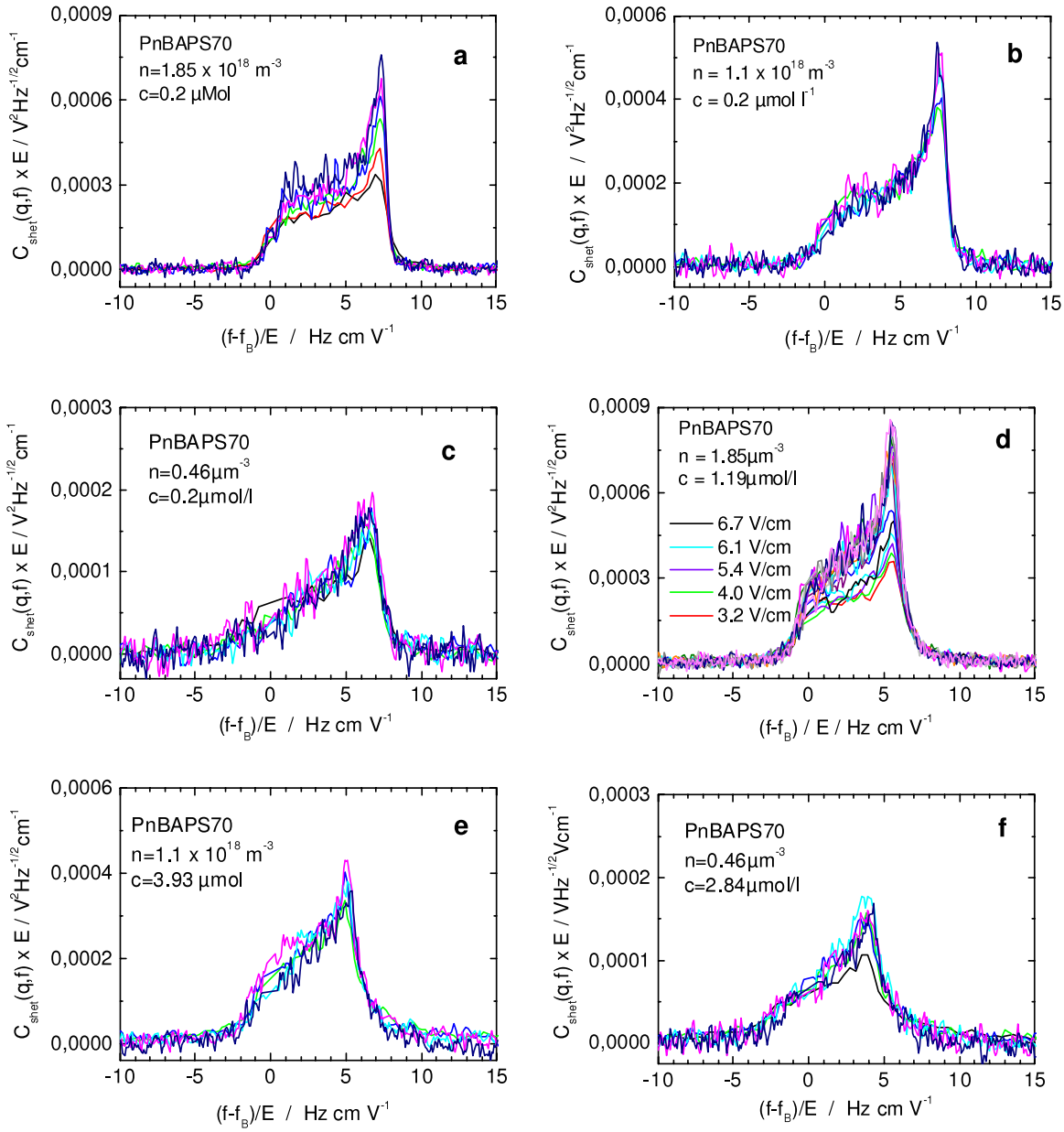

Figure 8. Scaled Doppler spectra of several strongly to weakly interacting particle suspensions of PnBAPS70 at particle number densities n and salt concentrations c as indicated and $q = 3.5\ \mu\text{m}^{-1}$. (a)–(c) Deionized. (d)–(f) With added CO_2 at concentrations as indicated. In the most concentrated systems, (a) and (d), an increase of the spectral density with the applied electric field is observed. All other spectra neatly coincide. For details see section 4.

The disordered state at very high dilution is considered in figure 9. Two examples of Doppler spectra taken on suspensions of the larger latex (figure 9(a)) and silica particles (figure 9(b)) are shown. The latex system is deionized, i.e. the particles have an extended electric double layer, while for the silica system salt was added. Furthermore, in the silica system there is the same surface chemistry for the wall and the particles. Again, the spectral form is well fitted and a velocity distribution at mid-plane height can be attributed. As will be discussed in detail in section 3.2, the electric field dependence of D_{eff} has nearly vanished for these samples and, in contrast to the case with overlapping double layers, we observe a significant difference between μ_{e} and μ_{eo}, irrespective of the surface chemistry.

3.2. Field-strength dependence of A and D_{eff}

3.2.1. General observations. The frequency integrated spectral density, A, is observed to either stay constant or increase with increasing electric field strength. This is illustrated in figure 10(a). The absolute values, and hence the slopes, are not comparable for the systems shown, as the optical parameters differed in the experiments on different particle species and the PnBAPS70 curves were shifted for clarity. For a given suspension, however, the optical

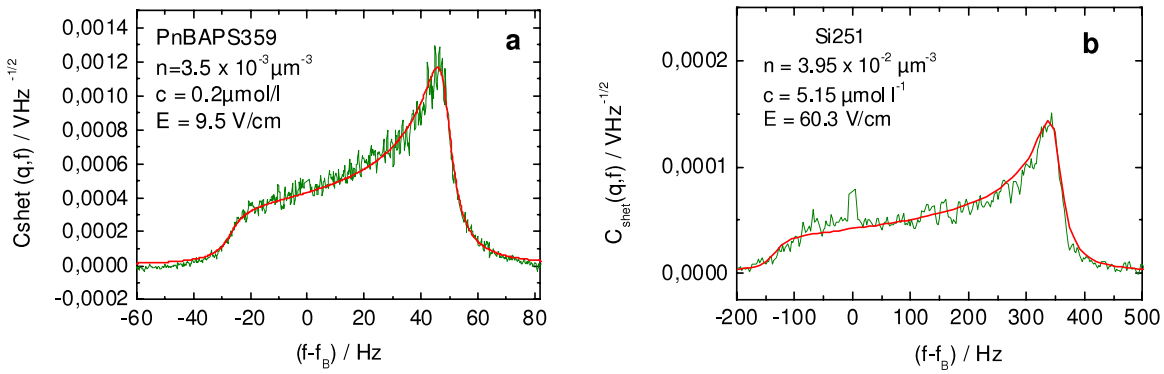

Figure 9. Bragg-shift-corrected Doppler spectra of non-interacting particle suspensions of (a) PnBAPS70 and (b) Si251, as obtained under deionized and salty conditions, measured at $q = 4.4\ \mu\text{m}^{-1}$ and fitted using equations (4)–(6) (red curve). Note the presence of strong electro-osmosis. Note further that in (b) the peak resulting from the beating of the reference beam light and parasitic stray light from the illumination beam at $f - f_B = 0$ was not corrected for.

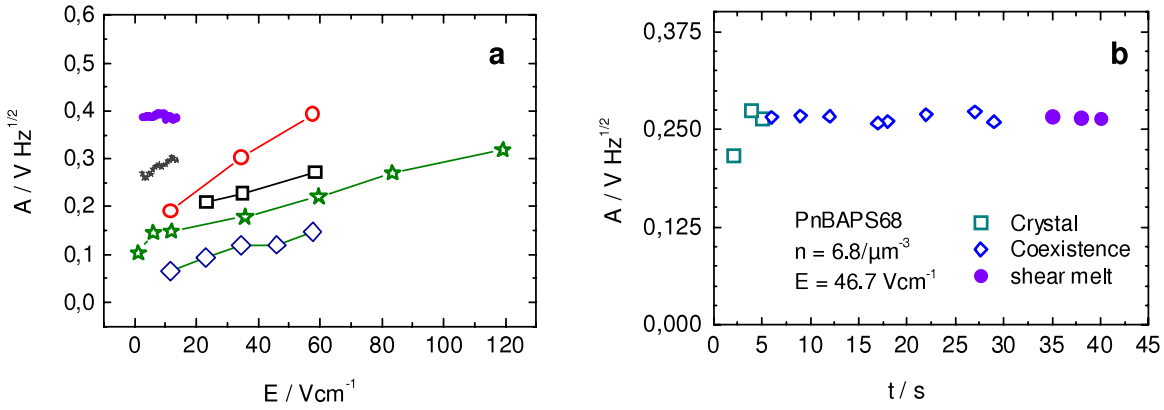

Figure 10. (a) Dependence of the frequency integrated spectral density, A, on the electric field strength, E, for different suspensions. Open symbols: deionized PnBAPS68; red circles: $n = 0.47\ \mu\text{m}^{-3}$ (fluid-like); black squares: $n = 4.7\ \mu\text{m}^{-3}$ (fluid-like); blue diamonds: $n = 5.8\ \mu\text{m}^{-3}$ (partially polycrystalline at $E = 11.7$ V cm^{-1}, shear molten at larger fields); green stars: $n = 26.5\ \mu\text{m}^{-1}$ (polycrystalline plug flow at low fields, wall-based oriented single crystals for large fields). Filled symbols: PnBAPS70; violet circles: $n = 0.46\ \mu\text{m}^{-3}$ and $c = 2.84\ \mu\text{mol l}^{-1}$ (very weakly interacting particle state); grey stars: $n = 1.85\ \mu\text{m}^{-3}$ and $c = 0.2\ \mu\text{mol l}^{-1}$ (fluid-like). All deionized systems show a significant increase of A with increasing field strength. In most cases the dependence is approximately linear. (b) Integrated spectral density, A, of deionized PnBAPS68 at $n = 6.8\ \mu\text{m}^{-3}$ and $E = 46.1$ V cm^{-1} during shear melting. The electric field was turned on at $t = 2$ s. After an initial jump, the integrated spectral intensity stays constant irrespective of the system structure. 400 spectra were taken over 40 s. The relative fluctuation between individual spectra never exceeded $\Delta A/A = \pm 0.1$ after turning on the electric field and no systematic variation with time was seen. The displayed data points are averaged over 1 s, i.e. over 10 spectra.

adjustment is kept and hence the qualitative field dependence can be studied without ambiguity.

In figure 10(a), A stays constant for salty systems at low particle concentrations (see also figures 11(a) and (b) and 12(d)). Also, deionized PnBAPS68 does not show a significant change of A at sufficiently low particle density. By contrast, fluid-like ordered systems show an increase. The increase appears to be approximately linear with the field. We further also addressed the electro-phoretic motion of crystalline systems. There, after application of an electric field for about a minute, a stationary state was always obtained in which the spectral form stayed constant. We typically observe that at low field strengths a (poly-)crystalline plug moves as a whole. At increased field strength the stationary state was either shear melted or showed a different crystal microstructure [24, 41, 64, 65]. Figure 10(a) shows data on A for both cases, i.e. for PnBAPS68 at $n = 5.8$ and $26.5\ \mu\text{m}^{-3}$.[3] The integrated spectral intensity increases with increasing field also for the (partially) crystalline systems. In a number of cases, e.g. for PnBAPS68 at $n = 26.5\ \mu\text{m}^{-3}$, a slowing increase is found.

In principle, a changed integrated spectral intensity of equilibrium crystalline samples could be directly coupled to a changed overall system structure, i.e. the shear melting transition or a change of the microstructure. The temporal evolution of the integrated spectral density, A, during the

[3] The original spectra can be found in [44]. There also A values are reported, which show the same field dependences, albeit at slightly different absolute values. These differences are due to different correction procedures. The data shown here in figure 10(a) refer to spectra which were background corrected and further corrected for the 2 kHz peak. The time dependent data presented for $n = 6.8\ \mu\text{m}^{-3}$ in figure 10(b) are taken from [66] and are evaluated from the raw spectra without background correction but with correction for the 2 kHz peak.

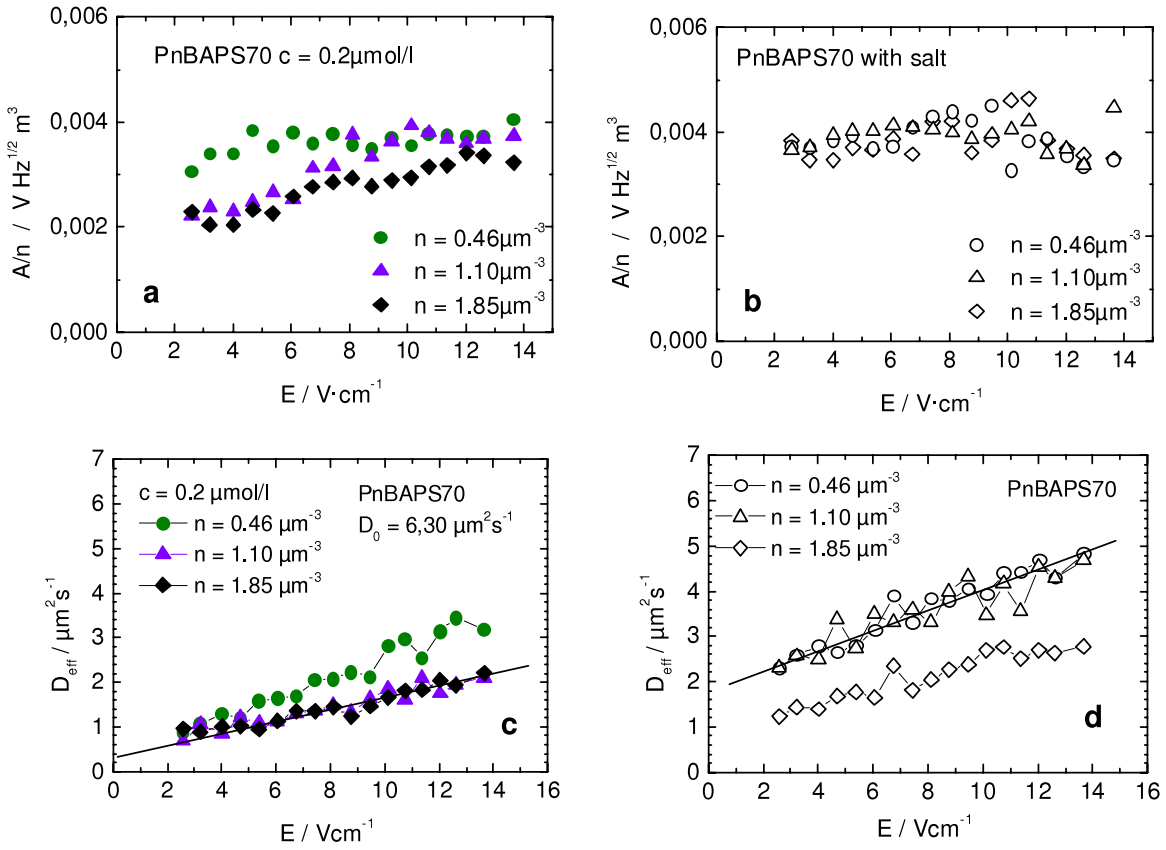

Figure 11. Fit results for moderately concentrated PnBAPS70 at various experimental conditions and $q = 3.5\ \mu\text{m}^{-1}$. (a) Field dependence of the integrated spectral density normalized to the indicated particle number densities, A/n, for PnBAPS70 under deionized conditions. (b) The same for salty samples of $c = 1.2\ \mu\text{mol l}^{-1}$ at $n = 0.46\ \mu\text{m}^{-3}$ (circles), $c = 3.9\ \mu\text{mol l}^{-1}$ at $n = 1.10\ \mu\text{m}^{-3}$ (triangles), and $c = 2.8\ \mu\text{mol l}^{-1}$ at $n = 1.85\ \mu\text{m}^{-3}$ (diamonds). (c) Field dependence of the effective diffusion coefficient, D_{eff}, for the samples in (a). (d) The same for the samples in (b), with symbols as before.

field-induced shear melting process is therefore investigated in figure 10(b) for an initially fully crystalline suspension of deionized PnBAPS68 at $n = 6.8\ \mu\text{m}^{-3}$. A field of $E = 46.1\ \text{cm}^{-1}$ was turned on at $t = 2$ s. After an initial jump, the integrated spectral density stays constant throughout the whole process of shear melting. The intensity increase as compared to the zero-field quiescent state is thus correlated to the presence and strength of the electric field. However, it is not influenced by the drastic change in the system structure on the scale of the inter-particle distance. Since further the increase in $I_{\text{shet}}(q, \omega)$ is spatially homogeneous, this observation allows the power spectra to be interpreted as particle velocity distributions irrespective of the phase state of the system. Therefore, flow-profiles become also accessible for crystalline [44] or partially shear molten states [67].

3.2.2. Quantitative analysis. For PnBAPS70 these measurements were repeated with great care taken to maintain identical illumination and detection conditions. The following quantitative analysis is restricted to a larger number of data points taken at rather low field strengths in the range of 2–14 V cm^{-1}. The results are displayed in figure 11. The large particle systems PnBAPS359 and Si251 can also be quantitatively evaluated, although there we do not have a large body of systematic data as yet. Results are shown in figure 12.

The data for the salty particle suspensions in figure 11(b) collapse onto a horizontal line, i.e. they are independent of E at values around $A/n \approx 0.004\ \text{VHz}^{1/2}\ \text{m}^3$. This confirms the theoretically expected scaling with n. Also for the considered very dilute, hardly correlated systems of larger particles, the field dependences of A in figures 12(a) and (c) are very weak, if not negligible.

For the deionized systems of PnBAPS70 a field dependence of A is found. For the two most strongly interacting suspensions values around $A/n \approx 0.002\ \text{V Hz}^{1/2}\ \text{m}^3$ are observed at low field strengths. With increasing field strength A/n begins to increase up to values close to those of the salty systems. As a trend, for the stronger particle correlation (more pronounced fluid-like order), the start of the increase is observed at larger electric field strength, and the increase displays a smaller slope. This trend is corroborated by the data for the deionized suspension at $n = 0.46\ \mu\text{m}^{-3}$ of weakly pronounced fluid-like order, which start increasing from an intermediate A/n-value and quickly obtain an approximately constant value again at $A/n \approx 0.04\ \text{VHz}^{1/2}\ \text{m}^3$.

A natural upper limit of the spectral power is given by $I_{\text{r}}\langle I_{\text{S}}(\mathbf{q})\rangle = I_{\text{r}} I_0 n \overline{f^2(q)}(9s^2 + 1)$, which is here reached for the non-interacting suspensions (cf figures 6(d)–(f)) and for the moderately strong interacting suspensions in the limit of large field strengths. The observed field-induced change

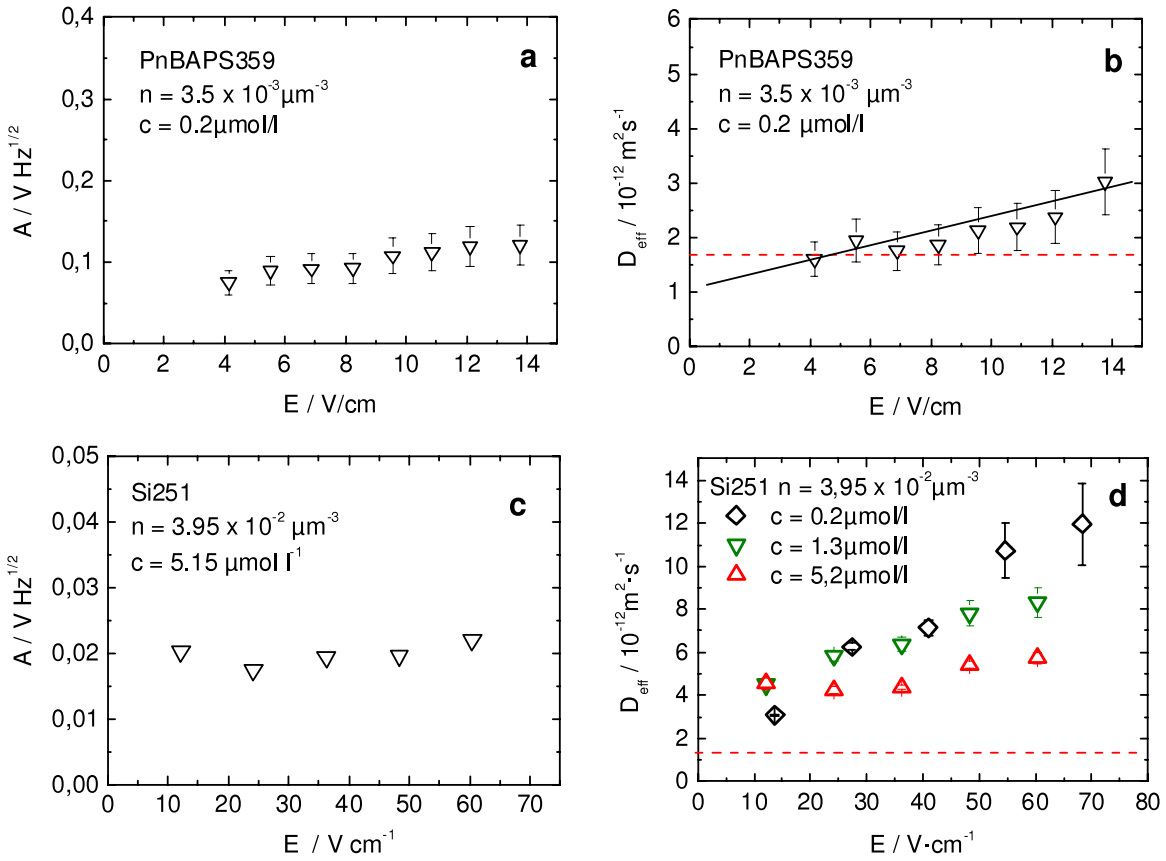

Figure 12. Fit results for very dilute large particle systems. (a), (b) Results for PnBAPS359 at deionized conditions and $q = 3.5\ \mu\text{m}^{-1}$; (c), (d) results for Si251 at salty conditions and $q = 4.4\ \mu\text{m}^{-1}$. (a), (c) The dependence of the integrated spectral density, A, on the applied electric field, E. The field dependence is weak for the deionized latex system and has practically vanished for the salty silica system. (b), (d) The field dependence of the effective diffusion coefficient, D_{eff}. The zero-field extrapolated value, $D_{\text{eff}}(E = 0)$, for the deionized latex particles is below the Stokes–Einstein value of $D_0 = 1.7 \times 10^{-12}\ \text{m}^2\ \text{s}^{-1}$ (dashed line). The solid straight line is a guide to the eye. For the silica system, the field dependence vanishes with increasing salt concentration, while $D_{\text{eff}}(E = 0)$ increases above its Stokes–Einstein value of $D_0 = 1.2 \times 10^{-12}\ \text{m}^2\ \text{s}^{-1}$.

of $S_{\text{M}}(\mathbf{q})$ is due to a change in the relative weight of coherent and incoherent contributions, i.e. to the increase of the interaction-monodisperse steady-state coherent structure factor, $S(q)$, with increasing field strength. We anticipate that the electric field induces density fluctuations on the probed length scale of a few inter-particle distances, which increase with increased field strength but are counteracted by the electrostatic interaction between the particles.

This interpretation does not necessarily disagree with the data in figure 10(a), where a linear increase of A is observed for the strongly interacting PnBA68-system over an extended range of field strengths, since we also here found that at strong electrostatic interactions the increase in A/n is linear at sufficiently low fields and only weak. Further, as mentioned above, the slopes in figure 10(a) cannot be evaluated quantitatively. The strongly interacting suspensions displayed there may therefore show a saturation behaviour at much larger fields than the suspensions investigated here at the transition from weak to moderately strong interactions.

In addition to the increase of the integrated spectral density, A, we also observe an increase of the effective diffusion coefficient, D_{eff}, with increasing field strength. Such an increase has been reported before, but only for one system under fixed interaction conditions [36]. Figures 11(c) and (d) quantify this increase for PnBAPS70 under different particle concentrations and salinities. In all cases, a linear increase is observed without any indication of a saturation effect. The extrapolated zero-field values are below the Stokes–Einstein value of $D_0 = 6.30 \times 10^{-12}\ \text{m}^2\ \text{s}^{-1}$. The slope of $D_{\text{eff}}(E)$ in figures 11(c) and (d) appears to be somewhat larger for the more strongly interacting systems. For the very dilute large particle systems in figures 12(b) and (d), we see that an increase is still present in the deionized latex system and the low-salt silica systems, but it is practically absent for the salty silica system. In all deionized systems, the zero-field extrapolated effective diffusion coefficients are smaller than the corresponding Stokes–Einstein value. For the very dilute silica system (cf figure 12(d)), $D_{\text{eff}}(E = 0)$ shows an increase with increasing salinity and becomes larger than D_0.

An increase in $D_{\text{eff}}(E = 0)$ with decreasing electrostatic interactions is expected. It corresponds to the transition in the dominant scattering contribution, from the incoherent self-intermediate scattering function, $G(\mathbf{q}, \tau)$, relating to self-diffusion, to the coherent steady-state dynamic structure factor, $S(\mathbf{q}, \tau)$, relating to collective diffusion. The observed field dependence, however, is not embodied in our simplified

analytic treatment based on equations (5)–(7) with D_0 replaced by $D_{\rm eff}$ as long as we assume $S(\mathbf{q}, \tau)$ to stay negligible also under an applied electric field. In fact, equation (7) predicts a field-strength independent diffusion coefficient, which is observed only for dilute systems of thin electric double layers.

Some alternative mechanisms suggested in the literature for a field dependent increase in $D_{\rm eff}$ [36] can be readily ruled out in our case. Joule heating, for instance, would vanish with decreasing salt concentration. Transient time broadening [68] should at the same velocity not depend on salinity and furthermore is negligibly weak at experimentally observed particle velocities of less than 10^3 μm s^{-1}. Several previous studies were concerned with the coupling of diffusion and/or density fluctuations to purely mechanical shear. Qiu *et al* [69] found a pronounced increase of the (anisotropic) long-time self-diffusion of non- or weakly interacting charged spheres under low frequency, oscillatory Couette flow. The enhancement in the direction of flow was attributed to Taylor dispersion [49]. The enhancement perpendicular to the flow direction was also theoretically investigated by Breedveld and Levine [70] and in Stokesian dynamics simulations of non-dilute sheared hard sphere systems [71]. For the collective diffusion of sheared hard spheres, the anisotropy is much less pronounced [72]. Not much is as yet known about suspensions of strongly interacting particles under shear, and in particular under electro-osmotically induced shear. Due to the overall parabolic flow-profile in the present experiments, however, we would in any case expect an inhomogeneous spatial distribution of observable effects. The effective diffusion should be enhanced at the cell wall where high shear rates are found, but remain unaltered in the cell centre at the tip of the parabola. This, however, could not be resolved within experimental uncertainty.

To rationalize our simultaneous observations of a spatially homogeneous field-enhanced spectral density and a field-enhanced effective diffusion coefficient, we rather favour an explanation based on a variation in the particle velocities in the presence of a homogeneous electric field. Such fluctuations could originate either from a mobility polydispersity, or from temporal fluctuations of the electrophoretic velocity, e.g. due to hydrodynamic interactions. Both kinds of velocity fluctuation have recently been addressed.

In a study on the electro-kinetics of charged spheres in a *quiescent* solvent, Araki and Tanaka [56] performed numerical calculations based on a so-called fluid particle dynamics (FPD) method, which accounts for many-particle hydrodynamic interactions. Still within the linear response regime of the field dependence of the electro-kinetic velocities, the authors found hydrodynamically induced velocity fluctuations. The magnitude of the fluctuations increases with increasing absolute drift velocity and thus with increasing field strength. Clearly, such fluctuations will directly mimic an enhanced diffusivity in the direction parallel to the drift velocity. For low field strengths, the velocity fluctuations decrease monotonically with increasing salinity. The authors further pointed out that these fluctuations significantly alter the pair correlation function, i.e. they translate into density fluctuations.

The case of a mobility polydispersity underlying our combined observations on A and $D_{\rm eff}$ was very recently addressed by Medebach [44]. He explicitly analysed the spectra of crystallized PnBAPS68 at deionized conditions and $n = 26.5$ μm^{-3}, where both an increase of integrated spectral density and a significant broadening of the plug-flow peak of that suspension are observed. Considering a mobility polydispersity but neglecting hydrodynamic coupling, the proposed theoretical model reproduced the slowing increase in $A(E)$ and the linear increase in $D_{\rm eff}(E)$.

From the present data we cannot clearly discriminate between these two approaches. However, both kinds of velocity fluctuation may easily mimic an increase of diffusion with increasing field strength. Furthermore they can couple to density fluctuations on scales slightly larger than the average inter-particle distance. They therefore may become visible in the present experiments at low scattering angles via a change in the measurable steady-state structure factor, $S_{\rm M}(q)$, and thus in $A(E)$. As the velocity fluctuations increase with increasing electric field strength, the spatial correlations vanish and $S(q)$ approaches unity.

3.3. Electro-kinetic mobilities

Earlier studies of colloidal electro-kinetics revealed a complex behaviour of the electro-phoretic mobility as a function of particle concentration. Using our combination of super-heterodyning with a reference beam setup, we gain additional insight by determining also the electro-osmotic mobility, $\mathbf{u}_{\rm eo} = \mu_{\rm eo}\mathbf{E}$. To the best of our knowledge, this study presents the first comparison of the two electro-kinetic mobilities measured for identical suspension parameters. Examples of both electro-kinetic velocities, as obtained for PnBAPS70, PnBAPS359 and Si251 from fitting the measured power spectra, are displayed in figures 13(a)–(d). In all studied cases, both electro-kinetic velocities, $\mathbf{u}_{\rm eo}$ and $\mathbf{v}_{\rm e}$, revealed a strictly linear dependence on E. This implies that all our experiments were performed in the regime of linear electro-kinetic response.

From these data, the electro-kinetic mobilities are derived from least-square linear fits. The results are displayed in figures 14(a) and (b) for the measurements on PnBAPS70 and PnBAPS359. For the deionized systems of PnBAPS70 in figure 14(a), $\mu_{\rm e}$ and $\mu_{\rm eo}$ are very close to each other with values of about 8.5 μm s^{-1} (V cm^{-1})$^{-1}$, with no systematic dependence on particle concentration. With added salt, the electro-osmotic mobilities of (7.5–8.2) μm s^{-1} (V cm^{-1})$^{-1}$ are somewhat smaller, but again they show no systematic dependence on the particle concentration. The electrophoretic mobilities of PnBAPS70 increase from a value of 4.0 μm s^{-1} (V cm^{-1})$^{-1}$ at $n = 0.47$ μm^{-3} to a value of 6.0 μm s^{-1} (V cm^{-1})$^{-1}$ at $n = 1.85$ μm^{-3}. For the deionized systems of PnBAPS359 in figure 14(b), the electro-osmotic mobility $\mu_{\rm eo} \approx 8.5$ μm s^{-1} (V cm^{-1})$^{-1}$ also appears to be independent of particle concentration at a value close to that observed in figure 14(a). The electro-phoretic mobility shows a rather weak increase with increasing particle concentration at values of $\mu_{\rm e} \approx 3.8$–4 μm s^{-1} (V cm^{-1})$^{-1}$.

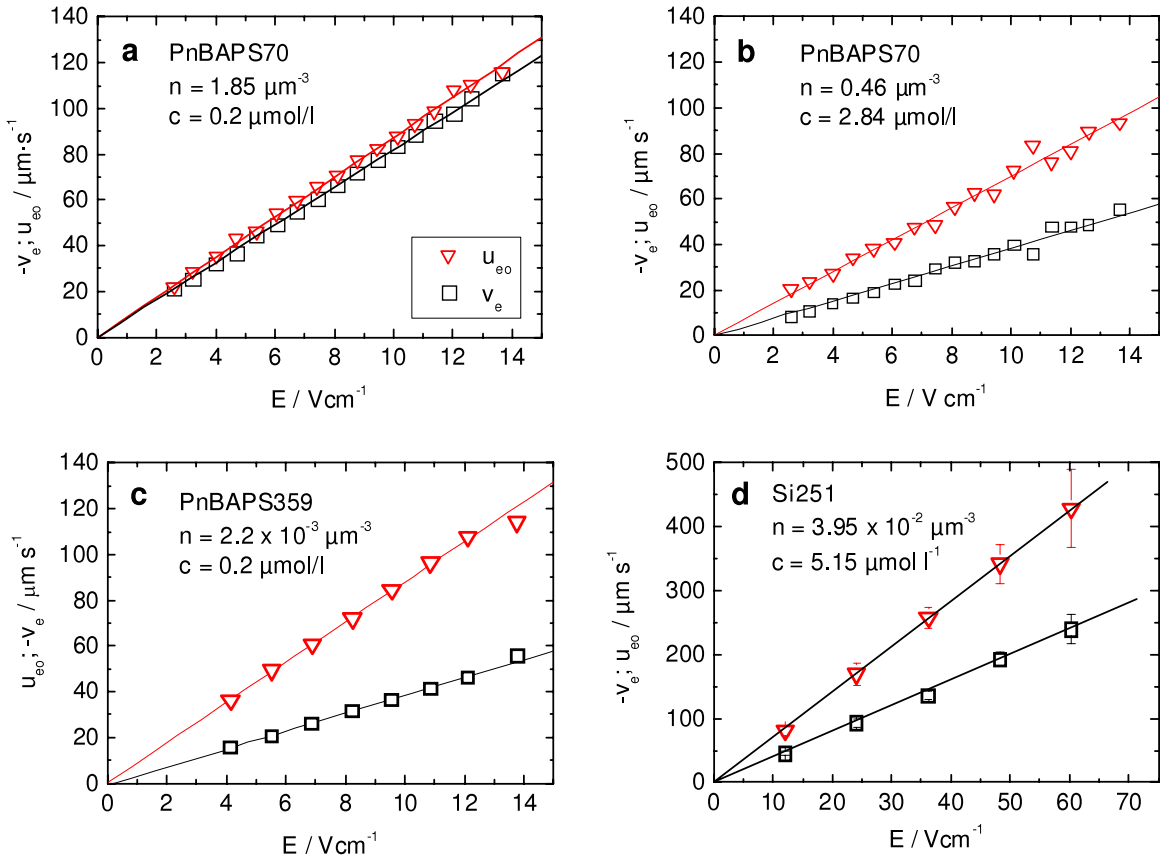

Figure 13. The electro-phoretic velocity, v_e (squares), and electro-osmotic velocity, u_{eo} (triangles), versus the strength of the applied electric field, E, for different systems as indicated. The lines are least-square fits to determine the corresponding mobilities. (a), (b) The results for the two PnBAPS70 samples with the strongest and weakest electrostatic interactions. The experimental parameters as indicated. (c), (d) The results for the highly dilute deionized latex and salty silica system of figure 12. Note that the electro-kinetic velocities nearly coincide in the strongly correlated case of (a) while for the other systems u_{eo} is considerably larger in magnitude than v_e.

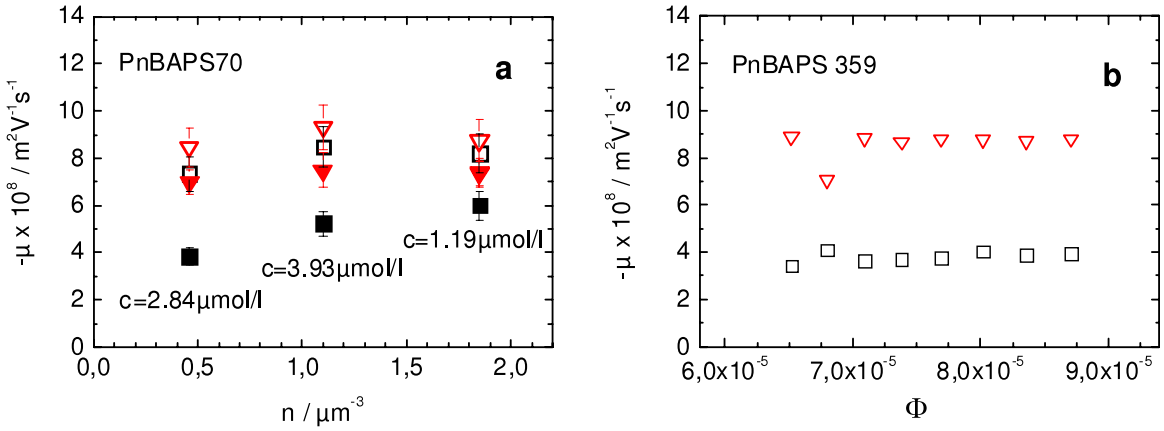

Figure 14. Electro-phoretic (squares) and electro-osmotic (down triangles) mobilities as a function of particle concentration. (a) PnBAPS70 under deionized conditions (open symbols) and with added CO_2 (closed symbols) at $c = 1.2$ μmol l^{-1} at $n = 0.46$ μm^{-3}, $c = 3.9$ μmol l^{-1} at $n = 1.10$ μm^{-3} and $c = 2.8$ μmol l^{-1} at $n = 1.85$ μm^{-3}. (b) PnBAPS359 under deionized conditions. The displayed volume fractions, $\Phi = (4\pi n)/(3a^3)$, correspond to number densities, n, of (2.7–3.6) $\times$ 10^{-3} μm^{-3}.

To compare absolute mobility values with systems of other particles and in other solvents, we can use the reduced mobility $\mu_{e,red} = (3/2)\eta\mu_e/\varepsilon_0\varepsilon_r k_B T$, where η is the solvent viscosity (0.97 cP for water), ε_0 and $\varepsilon_r = 80$ are the dielectric permittivities of vacuum and water, and $k_B T$ denotes the thermal energy. The plateau values of $\mu_{e,red}$ for deionized PnBAPS70 under strongly interacting conditions are slightly larger than the values reported for other deionized systems, which range between 4.5 and 6.5 μm s^{-1} (V cm^{-1})$^{-1}$ [16, 21]. The plateau values for the salty particle suspensions

of PnBAPS70 are slightly smaller, but again close to the values reported for other systems [16, 33]. The remaining quantitative differences are attributed to the different surface chemistries of the different particle species. The value of $\mu_{e,red} \approx 3.1$ for the highly dilute systems of PnBAPS359 and Si251 is larger than the value of 2 μm s^{-1} (V cm^{-1})$^{-1}$ obtained for a large number of measurements on strictly isolated spheres under deionized or low-salt conditions in water or water/glycerol mixtures [17–19]. Presumably the present experiment has not yet reached the limit of strictly non-interacting particles.

Also the observed dependence of the electro-phoretic mobility on particle concentration is consistent with earlier experimental observations made on other systems in [20–22, 33]. We observe a crossover from the regime of particle-concentration-independent electro-phoretic mobilities at strong electrostatic interactions to the concentration-dependent electro-phoretic mobilities at weaker to vanishing electrostatic interactions. We tried to correlate this crossover to the concentration dependence of other quantities. As already observed in earlier studies [33], the concentration of mobile counter-ions, nZ_{eff}, with the effective particle charge, Z_{eff}, taken from conductivity experiments amounts to ca. 1% of the total ion concentration in the crossover region. At the same time, the height of the principal peak of the corresponding measurable static structure factors, $S_M(q)$, is in the range of 1.6–1.2. These comparisons suggest that the crossover from particle-concentration-dependent mobilities to concentration-independent mobilities is correlated to the onset of fluid-like order for increasingly overlapping electric double layers rather than to a dominance of counter-ion screening.

By contrast to μ_e, the electro-osmotic mobility does not show any significant variation with increasing n. We thus observe a remarkable trend. At strongly interacting particle conditions we find a coincidence of electro-phoretic and electro-osmotic velocity values (figures 6 and 13(a)), while with decreasing interaction the electro-phoretic mobility drops below the electro-osmotic mobility which remains at a large value. This different behaviour is unlikely to originate from differences in the surface chemistry, since it is also observed for the Si251 particle suspensions (cf figure 12(d)), where both the spheres and the wall are made of silica and share the same surface chemistry and sample preparation protocol. Possibly, our observations indicate an influence of the different geometries of the charged surfaces. Even at identical bare charge density for chemically identical surfaces, the amount of counter-ion condensation will show a different behaviour upon dilution for spheres and planar walls [25–28][4]. However, we refrain from any speculation until systematic and comprehensive data are available covering the full range of interesting particle concentrations for the same particle species. Corresponding experiments are currently under way for several silica systems.

[4] In essence, upon dilution and loss of double layer overlap the condensed counter-ions will partially evaporate from the surface of a sphere, while for a planar wall the amount of counter-ion condensation is unaffected by dilution. Therefore both the spheres and the walls possess a similar layer of condensed counter-ions under conditions of strong overlap of the electric double layers. By contrast, under less overlapping conditions this condensed layer is reduced for spheres but kept essentially constant for the planar walls.

4. Discussion

In this paper, we have demonstrated the versatility and facility of a new Doppler velocimetry instrument for measurements of electro-kinetic properties of suspensions of strongly interacting and highly correlated charged particles. In particular, we were able to extract the mobility, μ_e, from the measured, dominantly incoherent, super-heterodyne reference beam integral spectra. Moreover, we could also quantify other important parameters characterizing the electro-kinetic flow properties of suspensions of charged particles, such as the electro-osmotic mobility, determining the solvent flow-profile, an effective particle diffusion coefficient, D_{eff}, and the integrated spectral density, A. This has been possible since our instrument is based on a straightforward combination of previous approaches, each contributing its own advantage. For instance, using super-heterodyning as originally introduced by [37, 38] we are able to discriminate the most interesting, purely heterodyne contribution to the Doppler spectra without the interference of the unwanted homodyne part or low frequency noise.

Further, the use of a reference beam integral measurement as originally reported in [36] allowed us to demonstrate the validity of the assumed electro-kinetic flow-profile with its slight deviations from an ideal parabolic shape, and we could exclude significant effects of shear thinning and/or particle density inhomogeneity. To the best of our knowledge, this is the first experimental verification of Komagata's analytical expression for the mid-plane flow-profile (equation (1)) for systems with strong electrostatic particle interactions and pronounced fluid-like order. The Komagata approximation for the case of crystalline systems remains to be explored, as there the particles do not follow the electro-osmotic flow-profile of the solvent. Over a large range of particle concentrations, we obtained high quality Doppler spectra which are well suited for further quantitative evaluation. In particular, we could simultaneously determine the electro-phoretic and electro-osmotic mobilities in a convenient way, from a single set of electric field dependent measurements at mid-plane height, irrespective of the strength of particle correlations.

An important experimental condition was given by the choice of the probed q-range. We adapted the conventional heterodyne light scattering theory to meet the experimental conditions of our new instrument. This will be presented in detail in a forthcoming paper [45]. From this theoretical work, we anticipate that for measurements performed at low q-values, smaller than the location of the principal peak of the static structure factor, the quantities D_{eff} and A would contain interesting additional information. In particular, the Doppler spectra recorded at such q-values and at low salinity are theoretically expected to be dominated by incoherently scattered light, due to the unavoidable optical polydispersity of colloidal particles and the low osmotic compressibility of strongly interacting suspensions [40]. The theoretical prediction was successfully tested at a small scattering angle

by following the behaviour of $D_{\text{eff}}(E = 0)$ over a large range of interaction conditions ranging from isolated, strongly screened particles to highly correlated, strongly interacting particles in fluid-like ordered suspensions. It was also probed by performing a shear melting experiment, during which the scattered intensity stayed constant, irrespective of the system structure. Hence, our instrument indeed dominantly probes the self-dynamics of the particle suspensions even in strongly interacting particle suspensions, and, in effect, it may be viewed as a tracer experiment without explicit tracers. This makes it particularly suited to the study of flow in suspensions with small but strongly interacting particles.

The electro-kinetic case studies presented here cover a large range of different strengths of particle interactions from systems close to freezing to very dilute and strongly screened systems. They revealed an interesting difference in the dependences of the two mobilities on the interaction conditions, which is at present not understood, but may be addressed by additional systematic measurements with our instrument. The simultaneously measured quantities D_{eff} and A further allowed us to characterize complementary aspects of the electro-kinetic flow behaviour. For isolated and electrostatically strongly screened particles in very dilute and/or salty suspension, we observe D_{eff} and A to be practically independent of the applied field strength. For deionized, but still very dilute, suspensions (i.e. for extended, but not yet overlapping, electric double layers) a linear dependence of the effective diffusion on the field strength is observed. Moving to more concentrated deionized suspensions (i.e. with the beginning of overlap of the electric double layers) we also find a field dependence of the integrated super-heterodyne spectral density suggesting the build-up of density fluctuations on the probed length scale. This increase occurs irrespective of the location of the scatterers within the cell. It is therefore not connected to the (locally varying) shear rate, in turn confirming the theoretically expected absence of significant Taylor dispersion in our electro-kinetic flow experiment [45]. Our investigations suggest a coupling of the self-dynamics, observed through D_{eff}, to particle density fluctuations on the scale of a few inter-particle distances observed through $A(E)$. To test this coupling, future studies should include a systematic determination of the q dependence of the observed increases in D_{eff} and A. Such a variation of scattering angle is already possible with the present instrument by employing different beam splitting gratings or by using a beam splitter as described in [36]. To verify the proposed velocity fluctuations and discriminate their nature, future experiments should be supplemented by further microscopic investigations providing complementary information on the involved mechanisms on the level of individual particles.

Another extension of the range of applicability may also be desirable. So far, the electro-phoretic mobility measurements in colloidal fluids and crystals, as well as a qualitative analysis of shear-induced phase transitions, was possible either for small particles or at comparably low volume fractions of large particles, where multiple scattering does not interfere. The proof of principle for an extension to multiple-scattering-free measurements has recently been given by Tagaki and Tanaka [73]. It should be easily feasible to adapt their local super-heterodyne illumination, detection and signal processing scheme for measurements at different cell depths to the integral approach employed here.

Finally, our approach is not restricted to electro-kinetic flows. Other flow situations, e.g. flow under hydrostatic pressure difference, can also be studied in suitable flow-through cells [67]. Such flows are known to display a 'catastrophic' decrease in suspension viscosity [74], due to shear melting including a concentric spatial distribution of coexisting phases [67, 75]. Also, in those cases, using an integral measurement across the complete cell depth and exploiting the dominance of the incoherent scattering contribution at low q would allow for convenient measurements of the flow behaviour irrespective of the local suspension structure.

5. Conclusion

The presented technique was shown to allow a comprehensive characterization of electro-kinetic flow in weakly to strongly interacting suspensions of different structures without the need to employ explicit tracers. With a few further modifications it can be applied to arbitrary flow situations in a straightforward way. As it gives access to several complementary quantities, it should be of great interest for studies on other model systems as well as biologic systems and/or industrial particle suspensions, whenever a comprehensive characterization of flows beyond an average flux is needed.

Acknowledgments

It is a pleasure to acknowledge the stimulating discussions we had with Wolfgang Paul, Vladimir Lobaskin, Felix Carrique, Mathieu McPhie and Martin Medebach. We further thank Martin Medebach for performing the measurements on PnBAPS68 and Nina Lorenz for providing the characterization of PnBAPS70. We also thank BASF AG, Ludwigshafen for particle supply. Financial support by the DFG (SFB TR6, project sections B1 and B2) and the Graduate School of Excellence, Mainz, is gratefully acknowledged. TK is a recipient of a fellowship through this Excellence Initiative (DFG/GSC 266).

References

[1] von Smoluchowski M 1903 *Bull. Int. Acad. Sci. Cracovie* 184
[2] Delgado A, González-Caballero F, Hunter R J, Koopal L K and Lyklema J 2007 *J. Colloid Interface Sci.* **309** 194
[3] O'Brien R W and White L R 1978 *J. Chem Soc. Faraday Trans.* II **74** 1607
[4] Dukhin S S and Derjaguin B V 1974 *Surface and Colloid Science* vol 7, ed E Matijevic (New York: Wiley) chapter 2
[5] O'Brien R W and Hunter R J 1981 *Can. J. Chem.* **59** 1878
[6] Henry D C 1948 *Trans. Faraday Soc.* **44** 1021
[7] Ohshima H 1994 *J. Colloid Interface Sci.* **168** 269

[8] Zukoski C F and Saville D A 1986 *J. Colloid Interface Sci.* **114** 32
Zukoski C F and Saville D A 1986 *J. Colloid Interface Sci.* **114** 45

[9] Mangelsdorf C S and White L R 1990 *J. Chem. Soc. Faraday Trans.* **86** 2859
Mangelsdorf C S and White L R 1998 *J. Chem. Soc. Faraday Trans.* **94** 2441
Mangelsdorf C S and White L R 1998 *J. Chem. Soc. Faraday Trans.* **94** 2583

[10] Carrique F, Arroyo F J and Delgado A V 2001 *J. Colloid Interface Sci.* **243** 351

[11] Carrique F, Arroyo F J and Delgado A V 2002 *J. Colloid Interface Sci.* **252** 126

[12] Carrique F, Arroyo F J, Jiménez M L and Delgado A V 2003 *J. Phys. Chem.* B **107** 3199

[13] Ohshima H 2006 *Theory of Colloid and Interfacial Electric Phenomena* (Amsterdam: Academic)

[14] Chiang C P, Lee E, He Y Y and Hsu J P 2006 *J. Phys. Chem.* B **110** 1490

[15] Carrique F and Ruiz-Reina E 2009 *J. Phys. Chem.* B **113** 8613

[16] Palberg T, Medebach M, Garbow N, Evers M, Barreira Fontecha A and Reiber H 2004 *J. Phys. Condens. Matter* **16** S4039

[17] Okubo T 1987 *Ber. Bunsenges. Phys. Chem.* **91** 1064

[18] Garbow N, Evers M and Palberg T 2001 *Colloids Surf.* A **195** 227

[19] Garbow N, Evers M, Palberg T and Okubo T 2004 *J. Phys.: Condens. Matter* **16** 3835

[20] Dunstan D E, Rosen L A and Saville D A 1992 *J. Colloid Interface Sci.* **153** 581

[21] Bellini T, Degiorgio V, Mantegazza F, Marsan F A and Scarneccia C 1995 *J. Chem. Phys.* **103** 8228

[22] Evers M, Garbow N, Hessinger D and Palberg T 1998 *Phys. Rev.* E **57** 6774

[23] Medebach M and Palberg T 2004 *J. Phys.: Condens. Matter* **16** 5653

[24] Medebach M, Shapran L and Palberg T 2007 *Colloid Surf.* B **56** 210

[25] Manning G S 1969 *J. Chem. Phys.* **51** 924
Manning G S 1969 *J. Chem. Phys.* **51** 3249

[26] Alexander S, Chaikin P M, Grant P, Morales G J, Pincus P and Hone D 1984 *J. Chem. Phys.* **80** 5776

[27] Belloni L 1998 *Colloids Surf.* A **140** 227

[28] Levin Y 2002 *Rep. Prog. Phys.* **65** 1577

[29] Hessinger D, Evers M and Palberg T 2000 *Phys. Rev.* E **61** 5493

[30] Medebach M *et al* 2005 *J. Chem. Phys.* **123** 104903

[31] Lobashkin V, Dünweg B, Holm C, Medebach M and Palberg T 2007 *Phys. Rev. Lett.* **98** 176105

[32] Carrique F and Ruiz-Reina E 2008 *J. Phys. Chem.* B **112** 11960

[33] Reiber H, Köller T, Palberg T, Carrique F, Ruiz-Reina E and Piazza R 2007 *J. Colloid Interface Sci.* **309** 315

[34] Gisler T, Schulz S F, Borkovec M, Sticher H, Schurtenberger P, D'Aguanno B and Klein R 1994 *J. Chem. Phys.* **101** 9924

[35] Trizack E and Levin Y 2004 *Phys. Rev.* E **69** 031403

[36] Palberg T and Versmold H 1989 *J. Phys. Chem.* **93** 5296

[37] Miller J F 1992 *J. Colloid Interface Sci.* **153** 266

[38] Miller J F, Schätzel K and Vincent B 1991 *J. Colloid Interface Sci.* **143** 532

[39] Härtl W and Versmold H 1984 *J. Chem. Phys.* **80** 1387

[40] Nägele G 1996 *Phys. Rep.* **272** 217

[41] Medebach M and Palberg T 2003 *J. Chem. Phys.* **119** 3360

[42] Happel J and Brenner H 1973 *Low Reynolds Number Hydrodynamics* (Leyden: Noordhoff International)

[43] Komagata S 1933 *Res. Electrotech. Lab. Tokyo Comm.* **348** 1

[44] Medebach M 2012 *J. Chem. Phys.* **136** 044201

[45] Nägele G, Schweinfurth H, Sieber B and Palberg T 2012 in preparation

[46] Berne B J and Pecora R 1990 *Dynamic Light Scattering* (Malabar, FL: Krieger) p 53

[47] Dhont J K G 1996 *An Introduction to the Dynamics of Colloids* (Amsterdam: Elsevier)

[48] Ware B R 1974 *Adv. Colloid Interface Sci.* **4** 1

[49] Taylor G I 1954 *Proc. R. Soc. Lond.* A **219** 186
Taylor G I 1954 *Proc. R. Soc. Lond.* A **223** 446

[50] Foister R T and van de Veen T G H 1980 *J. Fluid Mech.* **96** 105

[51] Fuller G G, Rallison J M, Schmidt R L and Leal L G 1980 *J. Fluid Mech.* **100** 555

[52] Derksen J and Van de Water W 1990 *Appl. Sci. Res.* **47** 221

[53] Busch S, Jensen T H, Chushkin Y and Fluerasu A 2008 *Eur. Phys. J.* E **26** 55

[54] Rusu D, Genoe D, van Puyvelde P, Peuvrel-Disdier E, Navard P and Fuller G G 1999 *Polymer* **40** 1353

[55] Salmon J B, Manneville S, Colin A and Pouligny B 2003 *Eur. Phys. J. Appl. Phys.* **22** 143

[56] Araki H and Tanaka H 2006 *Europhys. Lett.* **82** 18004

[57] Semwogerere D and Weeks E R 2008 *Phys. Fluids* **20** 043306

[58] Laun H M, Bung R, Hess S, Loose W, Hess O, Hahn K, Hädicke E, Hingmann R, Schmidt F and Lindner P 1993 *J. Rheol.* **36** 1057

[59] Rastogi S R, Wagner N J and Lustig S R 1996 *J. Chem. Phys.* **104** 9234

[60] Wette P, Schöpe H J and Palberg T 2009 *Phys. Rev.* E **80** 021407

[61] Palberg T, Härtl W, Wittig U, Versmold H, Würth M and Simnacher E 1992 *J. Phys. Chem.* **96** 8180

[62] Wette P, Schöpe H-J, Biehl R and Palberg T 2001 *J. Chem. Phys.* **114** 7556

[63] Lobaskin V, Dünweg B and Holm C 2004 *J. Phys.: Condens. Matter* **16** S4063

[64] Medebach M and Palberg T 2003 *Colloid Surf.* A **222** 175

[65] Medebach M and Palberg T 2003 *J. Chem. Phys.* **119** 3360

[66] Medebach M 2004 Elektrokinetik konzentrierter kolloidaler suspensionen *PhD Thesis* University of Mainz

[67] Palberg T and Würth M 1996 *J. Physique* I **6** 237

[68] Edwards R V, Angus J C, French M J and Dunning J W Jr 1971 *J. Appl. Phys.* **42** 837

[69] Qiu X, Daniel-Ou-Yang H, Pine D J and Chaikin P M 1988 *Phys. Rev. Lett.* **61** 2554

[70] Breedveld V and Levine A J 2003 *Soft Mater.* **1** 235

[71] Foss D R and Brady J F 1999 *J. Fluid Mech.* **401** 243

[72] Leshansky A M, Morris J F and Brady J F 2008 *J. Fluid Mech.* **597** 305

[73] Tagaki S and Tanaka H 2010 *Phys. Rev. Lett.* **81** 021401

[74] Chen L B and Zukoski C F 1990 *J. Chem. Soc. Faraday Trans.* **86** 2629
Chen L B and Zukoski C F 1990 *Phys. Rev. Lett.* **65** 44

[75] Palberg T and Streicher K 1994 *Nature* **367** 51